

Exploring the interplay between mass-energy equivalence, interactions and entanglement in an optical lattice clock

Anjun Chu,^{1,2,*} Victor J. Martínez-Lahuerta,³ Maya Miklos,¹ Kyungtae Kim,¹

Peter Zoller,^{4,5} Klemens Hammerer,³ Jun Ye,¹ and Ana Maria Rey^{1,2}

¹*JILA, NIST and Department of Physics, University of Colorado, Boulder, Colorado 80309, USA*

²*Center for Theory of Quantum Matter, University of Colorado, Boulder, Colorado 80309, USA*

³*Institut für Theoretische Physik, Leibniz Universität Hannover, Appelstraße 2, 30167 Hannover, Germany*

⁴*Institute for Quantum Optics and Quantum Information of the Austrian Academy of Sciences, 6020 Innsbruck, Austria*

⁵*Institute for Theoretical Physics, University of Innsbruck, 6020 Innsbruck, Austria*

(Dated: June 7, 2024)

We propose protocols that probe manifestations of the mass-energy equivalence in an optical lattice clock (OLC) interrogated with spin coherent and entangled quantum states. To tune and uniquely distinguish the mass-energy equivalence effects (gravitational redshift and second order Doppler shift) in such setting, we devise a dressing protocol using an additional nuclear spin state. We then analyze the interplay between photon-mediated interactions and gravitational redshift and show that such interplay can lead to entanglement generation and frequency synchronization. In the regime where all atomic spins synchronize, we show the synchronization time depends on the initial entanglement of the state and can be used as a proxy of its metrological gain compared to a classical state. Our work opens new possibilities for exploring the effects of general relativity on quantum coherence and entanglement in OLC experiments.

Introduction.—Understanding the interplay between quantum mechanics (QM) and general relativity (GR) is a fundamental quest for modern science. Nevertheless up to date, measurements capable of genuinely witnessing this simultaneous interplay have not been realized in tabletop experiments. A push forward towards this milestone is becoming feasible thanks to recent improvements in precision and accuracy of atomic clocks and interferometers, including matter-wave tests of GR [1–7], the resolution of the gravitational redshift using spatially separated clocks [8, 9], and more recently within a millimeter-scale sample [10, 11]. These developments [1, 12] open up unique opportunities to search for new physics that could help reconcile the seemingly contradictory predictions of QM and GR.

Experimental developments have in parallel driven a great deal of theoretical effort towards the understanding of quantum dynamics with GR corrections. These progresses encompass analyses of relativistic corrections to Hamiltonians considered specifically in the context of neutral-atom and trapped-ion systems [13–26], tests of mass-energy equivalence with atoms in internal superposition states including predictions of energy-dependent phase shifts, loss of coherence and spin-motion coupling induced by gravitational time dilation [27–32], among others [33–39]. However, understanding the direct consequence of GR effects in more complex scenarios such as many-body systems, where particles can interact over the entire array, remains an outstanding problem.

In this work, we provide a first step in this direction by proposing near-term protocols to explore the manifestations of the leading order single-atom GR corrections in quantum many-body dynamics, taking advantage of the state-of-the-art Wannier-Stark OLCs with an array

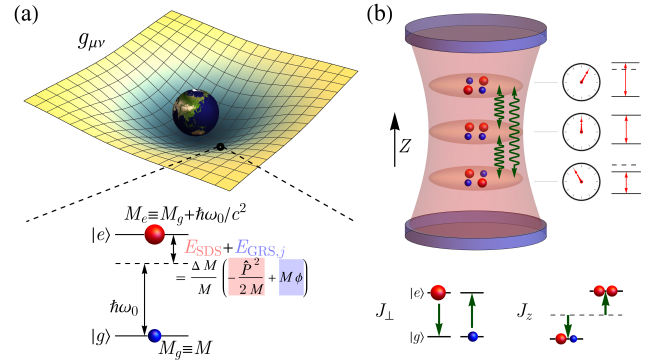


FIG. 1. (a) Schematic of an optical lattice clock (OLC) embedded in the curved spacetime (metric $g_{\mu\nu}$) formed by the earth’s gravity. Mass-energy equivalence is the leading order GR correction that translates internal energy difference $\hbar\omega_0$ between $|e\rangle$ and $|g\rangle$ states into a difference in the rest mass of an atom $\hbar\omega_0/c^2$. Such type of correction generates second-order Doppler shift E_{SDS} and gravitational redshift $E_{GRS,j}$ to the clock transition (see Eq. (3) and Eq. (4)). (b) Schematic of the interplay between gravitational redshift and collective cavity-mediated interactions (see Eq. (5)), with J_{\perp} and J_z collective exchange and Ising couplings.

of fully controllable interacting particles under gravity [10, 40]. We perform a detailed analysis of the effects of mass-energy equivalence in a clock transition, i.e. net change in relativistic rest mass due to internal energy, including the gravitational redshift and the second-order Doppler shift. We devise a dressing protocol using an additional nuclear spin state that can be used to tune and uniquely distinguish mass-energy equivalence in an OLC. Taking advantage of the dressing protocol, we further analyze the interplay between photon-mediated interactions

and the gravitational redshift acting on individual atoms. While gravitational redshift is akin to a mere level shift due to a magnetic field gradient, the observation in future OLCs will provide a direct test of GR effects acting on a many-body system. Depending on the relative strength of the redshift compared to a many-body energy gap induced by interactions, the system can feature local or global synchronization, as well as entanglement generation for both cases. For the latter case, we show that the synchronization time depends on the entanglement of the initial state and can be used as a proxy for the state's metrological utility.

Mass-energy equivalence in OLCs.—We consider a single atom in earth's gravity described by a curved space-time metric $g_{\mu\nu}$ (see Fig. 1(a)). We perform post-Newtonian expansion of $g_{\mu\nu}$ in power series of ϕ/c^2 [41, 42], with $\phi \approx gZ$ the Newtonian gravitational potential near the earth's surface and g the local gravitational acceleration. Following the treatment in Ref. [13, 16, 18, 21], one can obtain a single-atom Hamiltonian \hat{H}_A accounting for the leading relativistic corrections:

$$\hat{H}_A = \hat{H}_{\text{point}} \left(M + \frac{\hat{H}_I}{c^2} \right) + O(c^{-4}). \quad (1)$$

Here, $\hat{H}_{\text{point}}(M) = Mc^2 + \hat{H}_0(M) + \hat{H}_{\text{other}}$ is the Hamiltonian of a point particle with mass M , $\hat{H}_0(M) = \hat{\mathbf{P}}^2/(2M) + M\phi$ contains the non-relativistic terms, and \hat{H}_{other} contains other GR corrections arising from motion and metric geometry corrections [42]. The key idea of Eq. (1) can be understood as the mass-energy equivalence, summarized by the replacement $M \rightarrow M + \hat{H}_I/c^2$ in \hat{H}_{point} . OLCs feature an ultranarrow optical transition (clock transition) between two long-lived electronic states (excited state $|e\rangle$, ground state $|g\rangle$), which is described by the internal Hamiltonian $\hat{H}_I = \hbar\omega_0|e\rangle\langle e|$, with ω_0 the clock transition frequency measured at the lab position $Z = 0$ (see Fig. 1(a)). Since in an OLC \hat{H}_I contains the largest observable energy scale compared to other terms, the mass-energy equivalence is the leading order GR correction. It translates into a difference in the rest mass of an atom in states $|e\rangle$ and $|g\rangle$: $M_g = M$, $\Delta M = M_e - M_g = \hbar\omega_0/c^2$. Note that the mass defect ΔM is not simply a fixed number, and its tunability (see Fig. 2) is an important tool to determine the relativistic origin of the mass defect.

We assume that in OLCs atoms are trapped in a magic-wavelength 1D lattice along the gravitational potential (Z axis), where $|e\rangle$ and $|g\rangle$ states experience the same potential, $V(Z) = V_Z \sin^2(k_L Z) + M\phi$ [10, 40]. Here V_Z is the lattice depth, k_L is the wave number of the lattice that sets the atomic recoil energy $E_R = \hbar^2 k_L^2 / 2M$ and lattice spacing $a_L = \pi/k_L$. Metric geometry can also lead to corrections to optical lattices [26], which are negligible in our case. In a tilted 1D lattice described by $V(Z)$, the motional eigenstates in the ground band

are the so-called Wannier-Stark (WS) states $|W_j\rangle$, with j the Z -lattice site index where the WS state is centered at. Assuming the radial degrees of freedom are also confined to the lowest ground state by an additional 2D lattice, with lattice depths $V_{X,Y}$, the eigenenergies of WS states are given by $E_j = Mga_L j + E_{\text{band}}$, where $E_{\text{band}} \approx \sum_{\alpha=X,Y,Z} E_R (\sqrt{V_\alpha/E_R} - 1/4)$ is the ground band zero-point energy. The GR corrections due to mass-energy equivalence is given by

$$\hat{H}_{\text{corr}} = \sum_j (E_{\text{GRS},j} + E_{\text{SDS}}) |e, W_j\rangle \langle e, W_j|, \quad (2)$$

with $E_{\text{GRS},j}$ the gravitational redshift (GRS) and E_{SDS} the second-order Doppler shift (SDS). Their orders of magnitude are discussed below for ^{87}Sr atoms.

Applying the mass-energy equivalence to the gravitational potential energy $M\phi$, we get the GRS (or gravitational time dilation),

$$E_{\text{GRS},j} = \frac{\Delta M}{M} \langle W_j | M\phi | W_j \rangle = \hbar\omega_0 \frac{ga_L j}{c^2}. \quad (3)$$

The GRS leads to a gradient of frequency shift across the lattice. For example, the fractional frequency difference for nearest-neighbor lattice sites is just 4.4×10^{-23} , while it is at the order of 10^{-19} for 1 mm spatial separation as recently observed [10, 11].

The contribution of mass-energy equivalence in the kinetic energy leads to a local modification of the zero-point energy known as SDS (or motional time dilation),

$$E_{\text{SDS}} = -\frac{\Delta M}{M} \frac{\langle W_j | \hat{\mathbf{P}}^2 | W_j \rangle}{2M} = -\frac{\hbar\omega_0}{2Mc^2} E_{\text{band}}. \quad (4)$$

The magnitude of E_{SDS} increases with the lattice depth. For example, a deep lattice with $V_{X,Y,Z} = 300E_R$ leads to fractional frequency shift -4.5×10^{-21} . Corrections in the kinetic energy can also lead to a modification of the WS wave functions for $|e\rangle$ atoms, while they play a negligible role compared to $E_{\text{GRS},j}$ and E_{SDS} .

Tuning and distinguishing GR effects.—In standard OLCs, the effects of GRS might be mimicked by a weak magnetic field gradient. To observe genuine GR effects, one approach is to simultaneously observe $E_{\text{GRS},j}$ and E_{SDS} in the same system. This should be possible in next-term OLCs by populating higher motional bands if the systematic uncertainty of lattice Stark shifts [43] is suppressed below 10^{-20} .

We propose an alternative approach to use dressed states as means to tune the mass defect ΔM and with it simultaneously change $E_{\text{GRS},j}$ and E_{SDS} . As shown in Fig. 2(a), we make use of the intrinsic multilevel structure in fermionic alkaline earth atoms with nuclear spin F . We apply a dressing beam with Rabi frequency Ω and detuning δ connecting $|e, m_F\rangle$ with $|g, m_F - 1\rangle$ states, leading to the dressed states, $|+\rangle = C_1|e, m_F\rangle + C_2|g, m_F - 1\rangle$, $|-\rangle = -C_2|e, m_F\rangle + C_1|g, m_F - 1\rangle$, where $C_1 = (1 -$

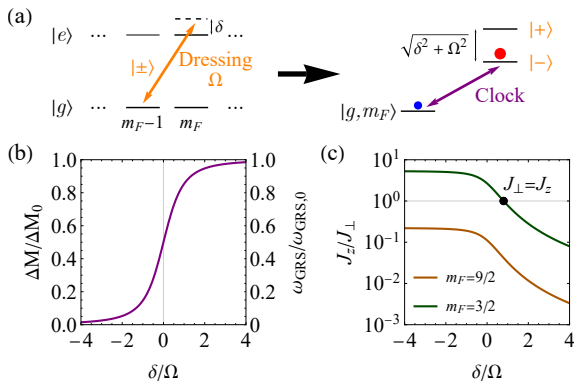


FIG. 2. Tuning mass-energy equivalence via dressed states. (a) Schematic of dressing the clock transition with another nuclear spin. The left panel show the application of the dressing laser, and the right panel show the new clock transition in the dressed basis. (b) The tunability of the mass defect ΔM and gravitational redshift ω_{GRS} as a function of dressing parameter δ/Ω . ΔM_0 and $\omega_{\text{GRS},0}$ are the corresponding values without dressing. (c) The tunability of cavity-mediated interactions (see \hat{H}_{cav} in Eq. (5)) as a function of dressing parameters δ/Ω and nuclear spin level m_F . Heisenberg interaction ($J_{\perp} = J_z$) can be reached with $m_F = 3/2$.

$\delta/\sqrt{\Omega^2 + \delta^2}^{1/2}/\sqrt{2}$, $C_2 = (1 + \delta/\sqrt{\Omega^2 + \delta^2})^{1/2}/\sqrt{2}$ in the rotating frame of the dressing laser. By addressing the transition between $|\uparrow\rangle \equiv |-\rangle$ and $|\downarrow\rangle \equiv |g, m_F\rangle$ states with a clock laser for the $\Delta m_F = 0$ transition, one can therefore get a tunable mass defect $\Delta M = |C_2|^2 \Delta M_0$ in the dressed clock transition via scanning the dressing parameter δ/Ω (see Fig. 2(b)), where $\Delta M_0 = \hbar\omega_0/c^2$ is the mass defect without the dressing laser. Since the nuclear spin states in the ground manifold share the same mass M but different Zeeman shifts [42], the dressing allows us to differentiate between a gravitational redshift and a magnetic field gradient. In the lab frame, we can understand the tunability of the mass-energy equivalence achieved by the dressing scheme by noticing that the state $|-\rangle$ has a probability $|C_2|^2$ to be in the $|e\rangle$ level and therefore an average internal energy of $|C_2|^2 \hbar\omega_0$.

This protocol is feasible thanks to the fact that the clock transitions between different nuclear spins are frequency resolved due to magnetic Zeeman shifts. We also assume all other dynamical frequencies are smaller than the dressed state energy gap $\sqrt{\Omega^2 + \delta^2}$ and the Zeeman shifts between nuclear spins. To guarantee the matching of laser phases for each atom, the dressing beam and the clock beam should be co-propagating. Moreover, spatial inhomogeneities in atomic detunings δ and in the dressing laser Rabi frequency Ω might obscure the effects of gravitational redshift. For a mHz gravitational redshift arising from a cm-scale spatial separation, it would be required to suppress the spatial variations of $\delta(Z)$, $\Omega(Z)$ and other source of perturbations below 10^{-4} Hz. This has already been achieved in Ref. [10] except the require-

ment for $\Omega(Z)$, which could be achievable using a cavity to stabilize the spatial mode of the dressing laser. One can also circumvent the stringent requirement for $\Omega(Z)$ by averaging the transition frequency of $|g, m_F\rangle \leftrightarrow |-\rangle$ and $|g, m_F\rangle \leftrightarrow |+\rangle$, while sacrificing the tunability of mass defect ($\Delta M = \Delta M_0/2$) [42].

Interplay with many-body dynamics.—After providing a recipe to distinguish genuine GR effects in OLCs, we further explore their manifestations in quantum many-body dynamics. We consider photon-mediated interactions generated by placing the atoms in an optical cavity [44, 45], in a regime where atomic contact interactions are controlled to be much weaker. The interplay between photon-mediated interactions and the GRS is described by the following Hamiltonian (see Fig. 1(b)):

$$\hat{H}_{\text{cav}}/\hbar = J_{\perp} \hat{\mathbf{S}} \cdot \hat{\mathbf{S}} + (J_z - J_{\perp}) \hat{S}^z \hat{S}^z + \omega_{\text{GRS}} \sum_j j \hat{S}_j^z, \quad (5)$$

where $\hbar\omega_{\text{GRS}} = (\Delta M)ga_L$ is the GRS between nearest neighbor sites, J_{\perp} and J_z are the collective exchange and Ising couplings. Here $\hat{S}_j^{x,y,z}$ are collective spin operators summed over all atoms at the same height ja_L , and $\hat{S}^{x,y,z} = \sum_j \hat{S}_j^{x,y,z}$. Based on Eq. (5), a magnetic field gradient will in principle give rise to similar single-atom inhomogeneities in the Hamiltonian. We drop the GR corrections for interaction terms since they are negligible in our case [42]. While the use of a single nuclear spin state restricts the cavity exchange interactions to a single polarization mode ($J_z = 0$ only), the dressing to another nuclear spin allows for coupling two polarization modes of the cavity [42], which enhances the tunability of \hat{H}_{cav} and realizes collective Heisenberg interactions ($J_{\perp} = J_z$) as shown in Fig. 2(c). In the following, we mainly focus on the case of $J_{\perp} = J_z$, since the $\hat{\mathbf{S}} \cdot \hat{\mathbf{S}}$ term becomes a constant and does not alter entanglement in the fully symmetric manifold. This requirement is unnecessary for observing frequency synchronization.

We propose to initialize all the atoms in the state $(|g\rangle + |e\rangle)/\sqrt{2}$, perform time evolution under Hamiltonian \hat{H}_{cav} (Eq. (5)), and then measure the phase shift of $\langle \hat{S}_j^+ \rangle$ for every Z -lattice site, resulting in frequency shift $\omega_j(t) = \tan^{-1} \left[\langle \hat{S}_j^y \rangle / \langle \hat{S}_j^x \rangle \right] / t$ as a function of evolution time (see Fig. 3(a)). It can be observed by the application of a $\pi/2$ pulse followed by local population measurements. Without interactions or in the case of short interrogation times, one expects to observe the GRS, $\omega_j = j\omega_{\text{GRS}}$, as reported in Ref. [10]. In the interaction dominated regime, the GRS persists only for a time scale shorter than the atomic interaction time scale. Beyond this period, the frequencies become synchronized due to interaction locking and reach $\omega_j \approx 0$ at synchronization time t_{syn} (see Fig. 3(b)). Without loss of generality, the numerical simulations in Fig. 3 and Fig. 4 are based on exact diagonalization for $N = 16$ atoms with one atom per Z -lattice site.

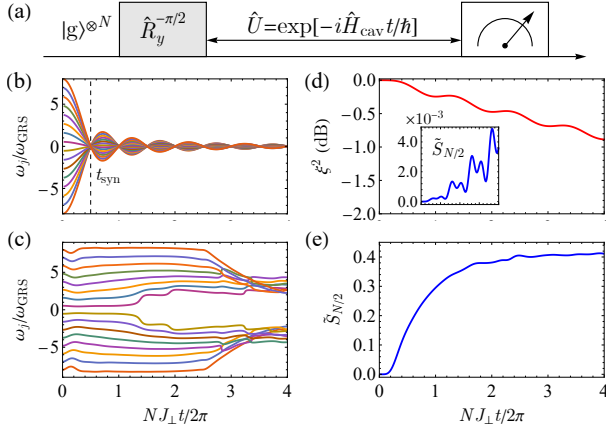


FIG. 3. Interplay between photon-mediated interactions and GRS. (a) We prepare a product state with all atoms in $|g\rangle$ state and apply a laser pulse $\hat{R}_y^{-\pi/2} = \exp(i\frac{\pi}{2}\hat{S}_y)$ to start the dynamics. We focus on a single chain with $N = 16$ atoms under the Hamiltonian \hat{H}_{cav} (Eq. (5)) with $J_{\perp} = J_z$. (b) Individual atomic frequency shift ω_j with $\omega_{split}/NJ_{\perp} = 0.3125$. Synchronization of atomic frequencies can be reached at time t_{syn} . (c) Individual atomic frequency shift ω_j with $\omega_{split}/NJ_{\perp} = 3.125$. Global synchronization fails to occur in this regime. (d) Spin squeezing parameter ξ^2 and normalized Rényi entropy $\tilde{S}_{N/2}$ (inset) in the case of (b). (e) Normalized Rényi entropy $\tilde{S}_{N/2}$ in the case of (c).

The emergent synchronization is the result of many-body gap protection also observed in prior experiments [44, 46–50], which arises when $\omega_{split} \ll \Delta E$. Here $\omega_{split} = (N_s - 1)\omega_{GRS}$ is the maximum redshift in the array, with N_s the number of lattice sites, and ΔE is the many-body gap due to Heisenberg couplings. On the contrary, in the regime $\omega_{split} \sim \Delta E$, the gap cannot maintain global synchronization (see Fig. 3(c)). Using a spin wave analysis one obtains $\Delta E = NJ_{\perp}$ and $NJ_{\perp}t_{syn} = \pi$ for $J_{\perp} = J_z$, where N corresponds to the total atom number in the array. For $N \sim 10^4 - 10^5$ ^{87}Sr atoms [44], one can achieve $NJ_{\perp}/2\pi \sim \text{Hz}$ ($\omega_{split}/NJ_{\perp} \sim 10^{-3}$ for cm-scale separation), leading to an achievable synchronization time scale in experiment.

Furthermore, we find that the simultaneous presence of single-atom GRS and photon-mediated interactions can lead to quantum entanglement as shown in Fig. 3(d,e). In fact, in the regime $\omega_{split} \ll \Delta E$, the projection of the wave function into the fully symmetric manifold imposed by the many-body gap transforms the single-particle term into an effective one-axis twisting (OAT) [51, 52] interaction term $\chi \hat{S}^z \hat{S}^z$, with $\chi \sim \omega_{split}^2/[N(\Delta E)]$ (see Ref. [53] where the splitting is generated by a different mechanism). In this case, entanglement builds up for $t > t_{syn}$, as witnessed by a squeezing parameter [52], $\xi^2 \equiv \min_{\varphi} N(\Delta S_{\varphi}^{\perp})^2/|\langle \hat{S} \rangle|^2 < 1$ (see Fig. 3(d)). Here, $(\Delta S_{\varphi}^{\perp})^2$ is the variance of spin noise along an axis perpendicular to the collective spin $\langle \hat{S} \rangle$. A faster growth

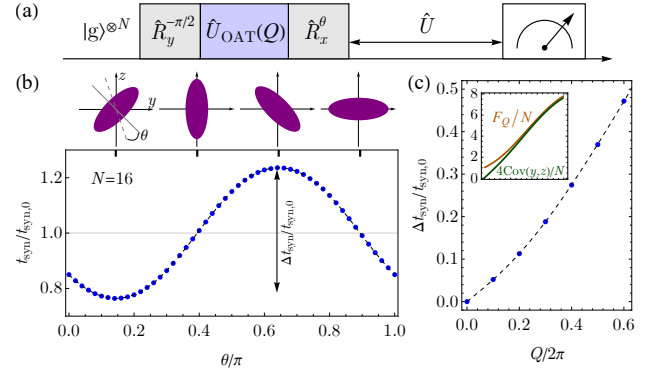


FIG. 4. Interplay between entanglement and GRS. (a) One-axis twisting (OAT) interactions $\hat{U}_{\text{OAT}}(Q) = \exp(-iQ\hat{S}^z\hat{S}^z/N)$ and rotations $\hat{R}_x^{\theta} = \exp(-i\theta\hat{S}^x)$ are first applied to generate a spin squeezed initial state (at $Q/2\pi = 0.6$), followed by unitary evolution under \hat{H}_{cav} . (b) The synchronization time, t_{syn} depends on the orientation of the spin squeezed state determined by θ . (c) Δt_{syn} (marked in (b)) as a function of OAT shearing strength Q . We show $4\text{Cov}(y, z)$ is approaching the quantum Fisher information F_Q for spin squeezed states (inset). We compare the numerical simulations (blue points) for $N = 16$ atoms under \hat{H}_{cav} ($J_{\perp} = J_z$) with Eq. (6) (black dashed lines).

of entanglement can be seen in the regime $\omega_{split} \sim \Delta E$ (see Fig. 3(e)). Since the entanglement in this case is not captured by spin squeezing, instead we characterize the entanglement by the normalized Rényi entropy $\tilde{S}_{N/2} = -\log_2(\text{tr}(\rho_{N/2}^2))/N$, where $\rho_{N/2}$ is the reduced density matrix by taking partial trace over half of the system. The entanglement builds up for $\omega_{split}t/2\pi > 1$ in this case, which might be due to population transfer to highly entangled states in manifolds of lower total spin [42]. For the implementation of entanglement generation, $\omega_{split}/NJ_{\perp} \sim 0.1 - 1$ is achievable for 10 cm – 1 m separation and $NJ_{\perp}/2\pi \sim 0.1$ Hz.

To study the effects of the GRS on quantum entanglement, we consider the scenario with entangled initial states, such as the ones generated using cavity induced OAT interactions [54, 55], $\hat{U}_{\text{OAT}}(Q) = \exp(-iQ\hat{S}^z\hat{S}^z/N)$, where Q is the shearing strength (Fig. 4(a)). The squeezing direction corresponds to the direction with minimum value of $(\Delta S_{\varphi}^{\perp})^2$, which can be controlled by performing a rotation $\hat{R}_x^{\theta} = \exp(-i\theta\hat{S}^x)$ as shown in Fig. 4. We assume the initial state preparation is fast enough such that the GRS does not play a role. We use $|\psi_0\rangle$ to denote the state after OAT interactions, and $|\psi(\theta)\rangle$ for the state after the \hat{R}_x^{θ} rotation.

In Fig. 4(b), we show that it is possible to control t_{syn} below or above the value of a product initial state $t_{syn,0}$ (obtained in Fig. 3) depending on the rotation \hat{R}_x^{θ} . The ratio $t_{syn}/t_{syn,0}$ under \hat{H}_{cav} ($J_{\perp} = J_z$) can be understood

using the following analytic result [42],

$$\frac{t_{\text{syn}}}{t_{\text{syn},0}} = 1 - \frac{2}{\pi} \arctan \left[\frac{\text{Cov}(y, z)}{(N-1)\langle \psi_0 | \hat{S}^x | \psi_0 \rangle} \right], \quad (6)$$

where $\text{Cov}(\alpha, \beta) \equiv \langle \psi(\theta) | (\hat{S}^\alpha \hat{S}^\beta + \hat{S}^\beta \hat{S}^\alpha) | \psi(\theta) \rangle - 2\langle \psi(\theta) | \hat{S}^\alpha | \psi(\theta) \rangle \langle \psi(\theta) | \hat{S}^\beta | \psi(\theta) \rangle$, with $\alpha, \beta = x, y, z$. The tunability of t_{syn} is due to the θ -dependence of $\text{Cov}(y, z)$. The tunable range $\Delta t_{\text{syn}} \equiv \max_\theta t_{\text{syn}} - \min_\theta t_{\text{syn}}$ can be used as a measure of entanglement (see Fig. 4(c)), since $4\text{Cov}(y, z)$ is approaching the quantum Fisher information F_Q [52], which corresponds to the maximal eigenvalue of the matrix $F_{Q,\alpha\beta} = 2\text{Cov}(\alpha, \beta)$.

Conclusion and outlook.—We discussed protocols accessible in OLCs that explore how the single-atom GR effects modify many-body dynamics generated by photon-mediated interactions. A similar interplay should be observable with atomic superexchange interactions [42]. While so far we have mostly focused on highly localized atomic arrays, generalizations to the case of itinerant particles where motion and other GR corrections also become relevant, will open unique opportunities for testing the basic tenets of GR when extended into the complex quantum domain.

We thank James Thompson, Raphael Kaubruegger, Dylan Young, Alexander Aepli, Michael Werner and Torsten Zache for useful discussions. This work is supported by the Sloan Foundation, the Simons Foundations and the Heising-Simons Foundation, NSF JILA-PFC PHY-2317149 and NSF OMA-2016244 (QLCI) grants, and by NIST.

* anjun.chu@colorado.edu

- [1] G. M. Tino, Testing gravity with cold atom interferometry: results and prospects, *Quantum Science and Technology* **6**, 024014 (2021).
- [2] S. Fray, C. A. Diez, T. W. Hänsch, and M. Weitz, Atomic interferometer with amplitude gratings of light and its applications to atom based tests of the equivalence principle, *Physical Review Letters* **93**, 240404 (2004).
- [3] H. Müller, A. Peters, and S. Chu, A precision measurement of the gravitational redshift by the interference of matter waves, *Nature* **463**, 926 (2010).
- [4] S.-Y. Lan, P.-C. Kuan, B. Estey, D. English, J. M. Brown, M. A. Hohensee, and H. Müller, A clock directly linking time to a particle's mass, *Science* **339**, 554 (2013).
- [5] M. Jaffe, P. Haslinger, V. Xu, P. Hamilton, A. Upadhye, B. Elder, J. Khoury, and H. Müller, Testing sub-gravitational forces on atoms from a miniature in-vacuum source mass, *Nature Physics* **13**, 938 (2017).
- [6] G. Rosi, G. D'Amico, L. Cacciapuoti, F. Sorrentino, M. Prevedelli, M. Zych, Č. Brukner, and G. M. Tino, Quantum test of the equivalence principle for atoms in coherent superposition of internal energy states, *Nature Communications* **8**, 15529 (2017).
- [7] P. Asenbaum, C. Overstreet, M. Kim, J. Curti, and M. A. Kasevich, Atom-interferometric test of the equivalence principle at the 10^{-12} level, *Physical Review Letters* **125**, 191101 (2020).
- [8] C.-W. Chou, D. B. Hume, T. Rosenband, and D. J. Wineland, Optical clocks and relativity, *Science* **329**, 1630 (2010).
- [9] M. Takamoto, I. Ushijima, N. Ohmae, T. Yahagi, K. Kokado, H. Shinkai, and H. Katori, Test of general relativity by a pair of transportable optical lattice clocks, *Nature Photonics* **14**, 411 (2020).
- [10] T. Bothwell, C. J. Kennedy, A. Aepli, D. Kedar, J. M. Robinson, E. Oelker, A. Staron, and J. Ye, Resolving the gravitational redshift across a millimetre-scale atomic sample, *Nature* **602**, 420 (2022).
- [11] X. Zheng, J. Dolde, M. C. Cambria, H. M. Lim, and S. Kolkowitz, A lab-based test of the gravitational redshift with a miniature clock network, *Nature Communications* **14**, 4886 (2023).
- [12] M. S. Safronova, D. Budker, D. DeMille, D. F. J. Kimball, A. Derevianko, and C. W. Clark, Search for new physics with atoms and molecules, *Review of Modern Physics* **90**, 025008 (2018).
- [13] F. E. Close and H. Osborn, Relativistic center-of-mass motion and the electromagnetic interaction of systems of charged particles, *Physical Review D* **2**, 2127 (1970).
- [14] K.-P. Marzlin, Dipole coupling of atoms and light in gravitational fields, *Physical Review A* **51**, 625 (1995).
- [15] S. Dimopoulos, P. W. Graham, J. M. Hogan, and M. A. Kasevich, General relativistic effects in atom interferometry, *Physical Review D* **78**, 042003 (2008).
- [16] M. Sonnleitner and S. M. Barnett, Mass-energy and anomalous friction in quantum optics, *Physical Review A* **98**, 042106 (2018).
- [17] V. Yudin and A. Taichenachev, Mass defect effects in atomic clocks, *Laser Physics Letters* **15**, 035703 (2018).
- [18] P. K. Schwartz and D. Giulini, Post-newtonian hamiltonian description of an atom in a weak gravitational field, *Physical Review A* **100**, 052116 (2019).
- [19] R. Haustein, G. J. Milburn, and M. Zych, Mass-energy equivalence in harmonically trapped particles, *arXiv:1906.03980* (2019).
- [20] S. Khandelwal, M. P. E. Lock, and M. P. Woods, Universal quantum modifications to general relativistic time dilation in delocalised clocks, *Quantum* **4**, 309 (2020).
- [21] V. J. Martínez-Lahuerta, S. Eilers, T. E. Mehlstäubler, P. O. Schmidt, and K. Hammerer, Ab initio quantum theory of mass defect and time dilation in trapped-ion optical clocks, *Physical Review A* **106**, 032803 (2022).
- [22] F. Di Pumpo, C. Ufrecht, A. Friedrich, E. Giese, W. P. Schleich, and W. G. Unruh, Gravitational redshift tests with atomic clocks and atom interferometers, *PRX Quantum* **2**, 040333 (2021).
- [23] P. T. Grochowski, A. R. H. Smith, A. Dragan, and K. Dębski, Quantum time dilation in atomic spectra, *Physical Review Research* **3**, 023053 (2021).
- [24] F. Di Pumpo, A. Friedrich, A. Geyer, C. Ufrecht, and E. Giese, Light propagation and atom interferometry in gravity and dilaton fields, *Physical Review D* **105**, 084065 (2022).
- [25] A. Alibabaei, P. K. Schwartz, and D. Giulini, Geometric post-newtonian description of massive spin-half particles in curved spacetime, *Classical and Quantum Gravity* **40**, 235014 (2023).
- [26] M. Werner, P. K. Schwartz, J.-N. Kirsten-Siemß, N. Gaaloul, D. Giulini, and K. Hammerer, Atom interfer-

- ometers in weakly curved spacetimes using bragg diffraction and bloch oscillations, *Phys. Rev. D* **109**, 022008 (2024).
- [27] M. Zych, F. Costa, I. Pikovski, and Č. Brukner, Quantum interferometric visibility as a witness of general relativistic proper time, *Nature Communications* **2**, 505 (2011).
- [28] I. Pikovski, M. Zych, F. Costa, and Č. Brukner, Universal decoherence due to gravitational time dilation, *Nature Physics* **11**, 668 (2015).
- [29] I. Pikovski, M. Zych, F. Costa, and Č. Brukner, Time dilation in quantum systems and decoherence, *New Journal of Physics* **19**, 025011 (2017).
- [30] M. Zych and Č. Brukner, Quantum formulation of the einstein equivalence principle, *Nature Physics* **14**, 1027 (2018).
- [31] A. Roura, Gravitational redshift in quantum-clock interferometry, *Physical Review X* **10**, 021014 (2020).
- [32] A. R. H. Smith and M. Ahmadi, Quantum clocks observe classical and quantum time dilation, *Nature Communications* **11**, 5360 (2020).
- [33] C. Marletto and V. Vedral, Gravitationally induced entanglement between two massive particles is sufficient evidence of quantum effects in gravity, *Physical Review Letters* **119**, 240402 (2017).
- [34] S. Bose, A. Mazumdar, G. W. Morley, H. Ulbricht, M. Toroš, M. Paternostro, A. A. Geraci, P. F. Barker, M. S. Kim, and G. Milburn, Spin entanglement witness for quantum gravity, *Physical Review Letters* **119**, 240401 (2017).
- [35] M. Zych, Ł. Rudnicki, and I. Pikovski, Gravitational mass of composite systems, *Physical Review D* **99**, 104029 (2019).
- [36] A. J. Paige, A. D. K. Plato, and M. S. Kim, Classical and nonclassical time dilation for quantum clocks, *Physical Review Letters* **124**, 160602 (2020).
- [37] D. Carney, H. Müller, and J. M. Taylor, Using an atom interferometer to infer gravitational entanglement generation, *PRX Quantum* **2**, 030330 (2021).
- [38] J. S. Pedernales, K. Streltsov, and M. B. Plenio, Enhancing gravitational interaction between quantum systems by a massive mediator, *Physical Review Letters* **128**, 110401 (2022).
- [39] M. Christodoulou, A. Di Biagio, M. Aspelmeyer, i. c. v. Brukner, C. Rovelli, and R. Howl, Locally mediated entanglement in linearized quantum gravity, *Physical Review Letters* **130**, 100202 (2023).
- [40] A. Aeppli, A. Chu, T. Bothwell, C. J. Kennedy, D. Kedar, P. He, A. M. Rey, and J. Ye, Hamiltonian engineering of spin-orbit-coupled fermions in a wannier-stark optical lattice clock, *Science Advances* **8**, eadc9242 (2022).
- [41] C. M. Will, *Theory and experiment in gravitational physics* (Cambridge university press, 2018).
- [42] See Supplemental Material at [URL will be inserted by publisher] for details of post-Newtonian corrections in an OLC, dressed state protocols, additional numerical simulations of superexchange interactions, as well as analytical derivation of synchronization time, includes Ref. [10, 13, 16, 18, 21, 26, 40, 41, 44, 56–62].
- [43] K. Kim, A. Aeppli, T. Bothwell, and J. Ye, Evaluation of lattice light shift at low 10^{-19} uncertainty for a shallow lattice sr optical clock, *Physical Review Letters* **130**, 113203 (2023).
- [44] M. A. Norcia, R. J. Lewis-Swan, J. R. Cline, B. Zhu, A. M. Rey, and J. K. Thompson, Cavity-mediated collective spin-exchange interactions in a strontium super-radiant laser, *Science* **361**, 259 (2018).
- [45] J. M. Robinson, M. Miklos, Y. M. Tso, C. J. Kennedy, T. Bothwell, D. Kedar, J. K. Thompson, and J. Ye, Direct comparison of two spin-squeezed optical clock ensembles at the 10^{-17} level, *Nature Physics* **20**, 208 (2024).
- [46] J. C. Allred, R. N. Lyman, T. W. Kornack, and M. V. Romalis, High-sensitivity atomic magnetometer unaffected by spin-exchange relaxation, *Physical Review Letters* **89**, 130801 (2002).
- [47] C. Deutsch, F. Ramirez-Martinez, C. Lacroûte, F. Reinhard, T. Schneider, J. N. Fuchs, F. Piéchon, F. Laloë, J. Reichel, and P. Rosenbusch, Spin self-rephasing and very long coherence times in a trapped atomic ensemble, *Physical Review Letters* **105**, 020401 (2010).
- [48] S. Smale, P. He, B. A. Olsen, K. G. Jackson, H. Sharum, S. Trotzky, J. Marino, A. M. Rey, and J. H. Thywissen, Observation of a transition between dynamical phases in a quantum degenerate Fermi gas, *Science Advances* **5**, eaax1568 (2019).
- [49] E. J. Davis, A. Periwal, E. S. Cooper, G. Bentsen, S. J. Evered, K. Van Kirk, and M. H. Schleier-Smith, Protecting spin coherence in a tunable Heisenberg model, *Physical Review Letters* **125**, 060402 (2020).
- [50] D. J. Young, A. Chu, E. Y. Song, D. Barberena, D. Wellnitz, Z. Niu, V. M. Schäfer, R. J. Lewis-Swan, A. M. Rey, and J. K. Thompson, Observing dynamical phases of bcs superconductors in a cavity qed simulator, *Nature* **625**, 679 (2024).
- [51] M. Kitagawa and M. Ueda, Squeezed spin states, *Physical Review A* **47**, 5138 (1993).
- [52] J. Ma, X. Wang, C.-P. Sun, and F. Nori, Quantum spin squeezing, *Physics Reports* **509**, 89 (2011).
- [53] P. He, M. A. Perlin, S. R. Muleady, R. J. Lewis-Swan, R. B. Hutson, J. Ye, and A. M. Rey, Engineering spin squeezing in a 3d optical lattice with interacting spin-orbit-coupled fermions, *Physical Review Research* **1**, 033075 (2019).
- [54] I. D. Leroux, M. H. Schleier-Smith, and V. Vuletić, Implementation of cavity squeezing of a collective atomic spin, *Physical Review Letters* **104**, 073602 (2010).
- [55] E. Pedrozo-Peñafiel, S. Colombo, C. Shu, A. F. Adiyatullin, Z. Li, E. Mendez, B. Braverman, A. Kawasaki, D. Akamatsu, Y. Xiao, *et al.*, Entanglement on an optical atomic-clock transition, *Nature* **588**, 414 (2020).
- [56] X. Zhang, M. Bishof, S. L. Bromley, C. V. Kraus, M. S. Safronova, P. Zoller, A. M. Rey, and J. Ye, Spectroscopic observation of su (n)-symmetric interactions in sr orbital magnetism, *Science* **345**, 1467 (2014).
- [57] G. F. Gribakin and V. V. Flambaum, Calculation of the scattering length in atomic collisions using the semiclassical approximation, *Physical Review A* **48**, 546 (1993).
- [58] A. Goban, R. B. Hutson, G. E. Marti, S. L. Campbell, M. A. Perlin, P. S. Julienne, J. P. D’incao, A. M. Rey, and J. Ye, Emergence of multi-body interactions in a fermionic lattice clock, *Nature* **563**, 369 (2018).
- [59] M. A. Perlin and A. M. Rey, Effective multi-body su (n)-symmetric interactions of ultracold fermionic atoms on a 3d lattice, *New Journal of Physics* **21**, 043039 (2019).
- [60] A. Piñeiro Orioli, J. K. Thompson, and A. M. Rey, Emergent dark states from superradiant dynamics in multi-level atoms in a cavity, *Physical Review X* **12**, 011054 (2022).
- [61] A. Chu, A. Piñeiro Orioli, D. Barberena, J. K. Thomp-

- son, and A. M. Rey, Photon-mediated correlated hopping in a synthetic ladder, [Physical Review Research](#) **5**, L022034 (2023).
- [62] W. R. Milner, S. Lannig, M. Mamaev, L. Yan, A. Chu, B. Lewis, M. N. Frankel, R. B. Hutson, A. M. Rey, and J. Ye, Coherent evolution of superexchange interaction in seconds long optical clock spectroscopy, [arXiv:2402.13398](#) (2024).

Exploring the interplay between mass-energy equivalence, interactions and entanglement in an optical lattice clock: Supplemental Materials

Anjun Chu,^{1,2} Victor J. Martínez-Lahuerta,³ Maya Miklos,¹ Kyungtae Kim,¹
Peter Zoller,^{4,5} Klemens Hammerer,³ Jun Ye,¹ and Ana Maria Rey^{1,2}

¹*JILA, NIST and Department of Physics, University of Colorado, Boulder, Colorado 80309, USA*

²*Center for Theory of Quantum Matter, University of Colorado, Boulder, Colorado 80309, USA*

³*Institut für Theoretische Physik, Leibniz Universität Hannover, Appelstraße 2, 30167 Hannover, Germany*

⁴*Institute for Quantum Optics and Quantum Information of the Austrian Academy of Sciences, 6020 Innsbruck, Austria*

⁵*Institute for Theoretical Physics, University of Innsbruck, 6020 Innsbruck, Austria*

(Dated: June 7, 2024)

S1. POST-NEWTONIAN CORRECTIONS

A. Post-Newtonian metric in the lab frame

Our starting point to include relativistic corrections is the parametrized post-Newtonian metric [S1–S4] in the isotropic coordinates (ct, x, y, z) ,

$$ds^2 = g_{\mu\nu} dx^\mu dx^\nu = -\left(1 + 2\frac{\bar{\phi}}{c^2} + 2\beta\frac{\bar{\phi}^2}{c^4}\right)c^2 dt^2 + \left(1 - 2\gamma\frac{\bar{\phi}}{c^2}\right)(dx^2 + dy^2 + dz^2) + O\left(\frac{1}{c^4}\right), \quad (\text{S1})$$

where $\bar{\phi}(R) = -GM_\oplus/R$ is the Newtonian gravitational potential of the earth, with M_\oplus the mass of the earth and $R = \sqrt{x^2 + y^2 + z^2}$. This metric agrees with the post-Newtonian expansion of Schwarzschild metric if $\beta = \gamma = 1$. Note that Eq. (S1) is reduced to Minkowski metric ($ds^2 = \eta_{\mu\nu} dx^\mu dx^\nu = -c^2 dt^2 + dx^2 + dy^2 + dz^2$) when $x, y, z \rightarrow \infty$.

Now we would like to define the lab frame, a reference frame which can be reduced to Minkowski metric at the lab position. First, we replace z by $R_\oplus + z$, with R_\oplus the earth's radius, so the lab position at the earth's surface is described by $x = y = z = 0$, where the radial direction is along the z axis. In this step, Eq. (S1) remains unchanged, and we can rewrite the gravitational potential as $\bar{\phi} = \phi_0 + \phi$, where $\phi_0 = \bar{\phi}(R_\oplus)$ is the gravitational potential at the earth's surface. Following Ref. [S4], we consider the following coordinate transformation,

$$T = \left(1 + \frac{\phi_0}{c^2} + \frac{2\beta - 1}{2} \frac{\phi_0^2}{c^4}\right)t, \quad X = \left(1 - \gamma\frac{\phi_0}{c^2}\right)x, \quad Y = \left(1 - \gamma\frac{\phi_0}{c^2}\right)y, \quad Z = \left(1 - \gamma\frac{\phi_0}{c^2}\right)z. \quad (\text{S2})$$

The lab frame can be described in terms of the new coordinates (cT, X, Y, Z) ,

$$ds^2 = -\left(1 + 2\frac{\phi}{c^2} + 2\beta\frac{\phi^2}{c^4} + 4(\beta - 1)\phi_0\frac{\phi}{c^4}\right)c^2 dT^2 + \left(1 - 2\gamma\frac{\phi}{c^2}\right)(dX^2 + dY^2 + dZ^2) + O\left(\frac{1}{c^4}\right). \quad (\text{S3})$$

Note that ϕ can be expanded as

$$\phi(Z) = gZ + O(Z^2), \quad (\text{S4})$$

where g is the gravitational acceleration. In the case of GR theory ($\beta = \gamma = 1$), the post-Newtonian metric in the two reference frames (see Eq. (S1) and Eq. (S3)) takes the same form, and this is the metric we used in the main text.

As a general remark, the gravitational redshift originates from the difference in the proper time $d\tau_p = ds/c$ for clocks at rest at different spatial coordinates due to the metric (see Eq. (S3)). If there is a single observer at a fixed position, the way to measure gravitational redshift is to send out laser beams with a unique frequency to different position, and the observer should find the difference of atomic transition frequency (clock) at different positions. If there are several observers at different positions, the way to measure gravitational redshift is to measure the frequency of the same laser beam at different positions assuming they have the same atomic transition frequency (clock), and they should observe different frequency for the light field. It is worth to mention that all the following discussions are based on the lab frame (see Eq. (S3)) defined here with a single observer at rest at the lab position.

B. Post-Newtonian single-atom quantum Hamiltonian

1. Key steps towards mass-energy equivalence

Post-Newtonian corrections for a quantum Hamiltonian can be determined in the following way [S2, S3]: Write down the classical action/Lagrangian in the lab frame consistent with GR, perform Legendre transformation to achieve the classical Hamiltonian, and then perform canonical quantization to achieve the quantum Hamiltonian. In the following, we will discuss the key idea of how mass-energy equivalence can be interpreted from the post-Newtonian corrections, and much more details can be found in Ref. [S2].

First we consider the post-Newtonian quantum Hamiltonian for a single free point particle with mass M . We start from the following classical action,

$$\mathcal{S}_{\text{point}} = -Mc \int dT \sqrt{g_{\mu\nu} \dot{x}^\mu \dot{x}^\nu}, \quad (\text{S5})$$

and the classical Lagrangian L_{point} is given by $\mathcal{S}_{\text{point}} = \int L_{\text{point}} dT$ in the lab frame (cT, X, Y, Z) . We have

$$\begin{aligned} L_{\text{point}} &= -Mc^2 \sqrt{-g_{\mu\nu} \dot{x}^\mu \dot{x}^\nu / c^2} \\ &= -Mc^2 + \frac{M\dot{\mathbf{X}}^2}{2} \left(1 + \frac{\dot{\mathbf{X}}^2}{4c^2}\right) - M\phi \left(1 + \frac{2\beta-1}{2} \frac{\phi}{c^2} + 2(\beta-1) \frac{\phi_0}{c^2}\right) - \frac{2\gamma+1}{2} \frac{M\phi}{c^2} \dot{\mathbf{X}}^2 + O\left(\frac{1}{c^4}\right), \end{aligned} \quad (\text{S6})$$

where $\dot{\mathbf{X}}^2 = \dot{X}^2 + \dot{Y}^2 + \dot{Z}^2$. The momentum \mathbf{P} is given by

$$\mathbf{P} = \frac{\partial L_{\text{point}}}{\partial \dot{\mathbf{X}}} = M\dot{\mathbf{X}} \left(1 + \frac{\dot{\mathbf{X}}^2}{2c^2} - (2\gamma+1) \frac{\phi}{c^2}\right) + O\left(\frac{1}{c^4}\right). \quad (\text{S7})$$

We use Legendre transformation to get the classical Hamiltonian, $H_{\text{point}} = \mathbf{P} \cdot \dot{\mathbf{X}} - L_{\text{point}}$, and then perform canonical quantization to achieve the quantum Hamiltonian,

$$\hat{H}_{\text{point}}(\hat{\mathbf{X}}, \hat{\mathbf{P}}, M) = Mc^2 + \hat{H}_0 + \hat{H}_{\text{other}}, \quad (\text{S8})$$

where \hat{H}_0 is the nonrelativistic Hamiltonian,

$$\hat{H}_0 = \frac{\hat{\mathbf{P}}^2}{2M} + M\phi, \quad (\text{S9})$$

and \hat{H}_{other} contains the relativistic corrections,

$$\hat{H}_{\text{other}} = -\frac{\hat{\mathbf{P}}^4}{8M^3c^2} + M\phi \left(\frac{2\beta-1}{2} \frac{\phi}{c^2} + 2(\beta-1) \frac{\phi_0}{c^2}\right) + \frac{2\gamma+1}{2} \frac{\hat{\mathbf{P}} \cdot \phi \hat{\mathbf{P}}}{Mc^2} + O\left(\frac{1}{c^4}\right). \quad (\text{S10})$$

For simplicity, we then consider the atom is formed by two charged particles interacting via EM fields, and there are no external EM fields coupled to the system. We also assume that the atom is a localized object such that the gravitational potential ϕ remains unchanged within the size of an atom. In the Coulomb gauge, one can finally reach the following atomic Hamiltonian [S2, S3],

$$\begin{aligned} \hat{H}_A &= \left(\sum_{n=1,2} M_n\right) c^2 + \sum_{n=1,2} \left[\frac{\hat{\mathbf{P}}_n^2}{2M_n} - \frac{\hat{\mathbf{P}}_n^4}{8M_n^3c^2} + M_n \phi \left(1 + \frac{2\beta-1}{2} \frac{\phi}{c^2} + 2(\beta-1) \frac{\phi_0}{c^2}\right) + \frac{2\gamma+1}{2} \frac{\hat{\mathbf{P}}_n \cdot \phi \hat{\mathbf{P}}_n}{M_n c^2} \right] \\ &+ \left(1 + (\gamma+1) \frac{\phi}{c^2}\right) \frac{e_1 e_2}{4\pi\epsilon_0 |\hat{\mathbf{X}}_{12}|} - \frac{e_1 e_2}{16\pi\epsilon_0 M_1 M_2 c^2} \left[\hat{\mathbf{P}}_1 \cdot \frac{1}{|\hat{\mathbf{X}}_{12}|} \hat{\mathbf{P}}_2 + \hat{\mathbf{P}}_1 \cdot \frac{(\hat{\mathbf{X}}_{12})(\hat{\mathbf{X}}_{12})}{|\hat{\mathbf{X}}_{12}|^3} \cdot \hat{\mathbf{P}}_2 + \text{h.c.} \right] + O\left(\frac{1}{c^4}\right), \end{aligned} \quad (\text{S11})$$

where $\hat{\mathbf{X}}_{12} = \hat{\mathbf{X}}_1 - \hat{\mathbf{X}}_2$. This Hamiltonian is the so-called Darwin Hamiltonian which includes relativistic corrections except the terms related to the electron spin. Here we would like to use this Hamiltonian as a toy model to discuss the relativistic corrections to the center-of-mass frame and the connection to the Hamiltonian of a point particle (see Eq.(S8)).

In the non-relativistic case, we define center-of-mass (COM) coordinates $(\hat{\mathbf{X}}', \hat{\mathbf{P}}')$ and internal coordinates $(\hat{\mathbf{x}}', \hat{\mathbf{p}}')$ in the following way,

$$\hat{\mathbf{X}}' = \frac{1}{M}(M_1\hat{\mathbf{X}}_1 + M_2\hat{\mathbf{X}}_2), \quad \hat{\mathbf{P}}' = \hat{\mathbf{P}}_1 + \hat{\mathbf{P}}_2, \quad \hat{\mathbf{x}}' = \hat{\mathbf{X}}_2 - \hat{\mathbf{X}}_1, \quad \hat{\mathbf{p}}' = \frac{M_1}{M}\hat{\mathbf{P}}_2 - \frac{M_2}{M}\hat{\mathbf{P}}_1, \quad (\text{S12})$$

where $M = M_1 + M_2$ is the total mass, and $\mu = M_1M_2/M$ is the reduced mass. However, if applying the coordinate transformation above to \hat{H}_A (see Eq. (S11)), one can easily find that it fails to separate the Hamiltonian into COM and internal degrees of freedom without crossed couplings. As proposed by Ref. [S5], one can apply relativistic corrections to the COM and internal coordinates using the following unitary transformation,

$$\hat{\mathbf{X}} = \hat{U}^\dagger \hat{\mathbf{X}}' \hat{U}, \quad \hat{\mathbf{P}} = \hat{U}^\dagger \hat{\mathbf{P}}' \hat{U}, \quad \hat{\mathbf{x}} = \hat{U}^\dagger \hat{\mathbf{x}}' \hat{U}, \quad \hat{\mathbf{p}} = \hat{U}^\dagger \hat{\mathbf{p}}' \hat{U}, \quad (\text{S13})$$

where

$$\hat{U} = \exp \left[i \frac{1}{4M^2c^2} \left((\hat{\mathbf{P}}' \cdot \hat{\mathbf{p}}')(\hat{\mathbf{P}}' \cdot \hat{\mathbf{x}}') + (\hat{\mathbf{P}}' \cdot \hat{\mathbf{x}}')(\hat{\mathbf{P}}' \cdot \hat{\mathbf{p}}') \right) + i \frac{M_1 - M_2}{4\mu M^2c^2} \left((\hat{\mathbf{p}}' \cdot \hat{\mathbf{p}}')(\hat{\mathbf{P}}' \cdot \hat{\mathbf{x}}') + (\hat{\mathbf{P}}' \cdot \hat{\mathbf{x}}')(\hat{\mathbf{p}}' \cdot \hat{\mathbf{p}}') \right) + i \frac{e_1 e_2 (M_1 - M_2)}{8\pi\epsilon_0 M^2 c^2} \frac{\hat{\mathbf{P}}' \cdot \hat{\mathbf{x}}'}{|\hat{\mathbf{x}}'|} \right]. \quad (\text{S14})$$

Using these new coordinates in Hamiltonian \hat{H}_A (see Eq. (S11)), we get

$$\hat{H}_A = \hat{H}_{\text{point}} \left(\hat{\mathbf{X}}, \hat{\mathbf{P}}, M + \frac{\hat{H}_I}{c^2} \right) + O(c^{-4}). \quad (\text{S15})$$

This is the so-called mass-energy equivalence since the atom Hamiltonian \hat{H}_A can be generated by replacing mass M by $M + \hat{H}_I/c^2$ in the point-particle Hamiltonian \hat{H}_{point} . In other words, the mass of a composite particle comprises the rest masses of the constituent particles as well as the internal energy. Here the internal Hamiltonian \hat{H}_I is given by

$$\hat{H}_I = \hat{H}_{I,0} + \hat{H}_{I,\text{SR}} + \hat{H}_{I,\text{GR}}, \quad (\text{S16})$$

where $\hat{H}_{I,0}$ is the non-relativistic internal Hamiltonian,

$$\hat{H}_{I,0} = \frac{\hat{\mathbf{p}}^2}{2\mu} + \frac{e_1 e_2}{4\pi\epsilon_0 |\hat{\mathbf{x}}|}, \quad (\text{S17})$$

$\hat{H}_{I,\text{SR}}$ contains the corrections due to special relativity,

$$\hat{H}_{I,\text{SR}} = -\frac{\hat{\mathbf{p}}^4}{8\mu^3 c^2} \frac{M_1^3 + M_2^3}{M^3} - \frac{e_1 e_2}{8\pi\epsilon_0 \mu M c^2} \left(\hat{\mathbf{p}} \cdot \frac{1}{|\hat{\mathbf{x}}|} \hat{\mathbf{p}} + \hat{\mathbf{p}} \cdot \frac{\hat{\mathbf{x}}\hat{\mathbf{x}}}{|\hat{\mathbf{x}}|^3} \cdot \hat{\mathbf{p}} \right) + O\left(\frac{1}{c^4}\right), \quad (\text{S18})$$

$\hat{H}_{I,\text{GR}}$ contains the corrections due to metric geometry,

$$\hat{H}_{I,\text{GR}} = \gamma \frac{\phi(\hat{\mathbf{X}})}{c^2} \left(\frac{\hat{\mathbf{p}}^2}{\mu} + \frac{e_1 e_2}{4\pi\epsilon_0 |\hat{\mathbf{x}}|} \right) + O\left(\frac{1}{c^4}\right). \quad (\text{S19})$$

2. List of relevant post-Newtonian correction terms

Here we list all the relevant post-Newtonian corrections terms for the single-atom Hamiltonian (see Fig. S1),

$$\hat{H}_{\text{sp}} = \hat{H}_A + \hat{H}_{AL}. \quad (\text{S20})$$

- \hat{H}_A is the atom Hamiltonian including center of mass and internal degrees of freedom. To the leading order of post-Newtonian expansion, we have \hat{H}_A given by Eq. (S15), with internal Hamiltonian \hat{H}_I (the case of two charged particles) given by Eq. (S16) and point-particle Hamiltonian \hat{H}_{point} given by Eq. (S8). To clearly indicate the post-Newtonian corrections, one can rewrite \hat{H}_A in the following form,

$$\hat{H}_A = Mc^2 + \hat{H}_0 + \hat{H}_I + \hat{H}_{\text{SDS}} + \hat{H}_{\text{GRS}} + \hat{H}_{\text{other}}. \quad (\text{S21})$$

We understand these corrections in the following way:

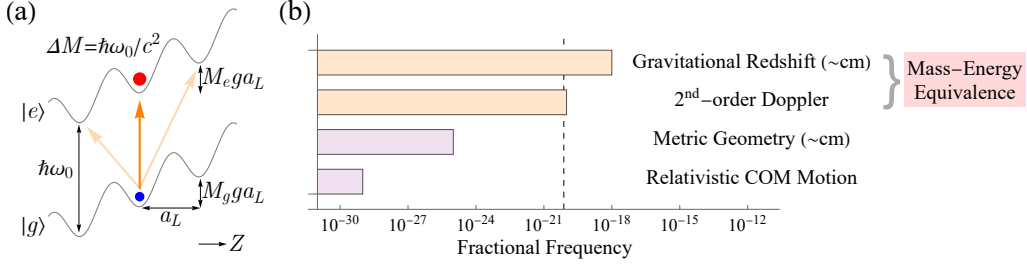


Fig. S1. (a) Schematic of an optical lattice clock with atoms trapped in a lattice tilted by gravity. Internal energy difference $\hbar\omega_0$ between $|e\rangle$ and $|g\rangle$ states can lead to mass difference ΔM in the Newtonian gravitational potential and generate gravitational redshift. It is possible to tune the frequency of laser beams to excite either on-site (orange arrow) or off-site (light orange arrows) transitions [S6, S7]. (b) Order of magnitude of the GR corrections for \hat{H}_A in fractional frequency of the clock transition (^{87}Sr). The light orange color marks the corrections due to mass-energy equivalence (see Eq. (S22) and Eq. (S23)), and the light purple color marks the other source of corrections (see Eq. (S10)). We assume MHz scale of kinetic energy and cm scale spatial separation of gravitational potential. The dashed line shows the current record of optical clock stability, 7.6×10^{-21} [S6].

1. Mass-energy equivalence. This is to replace M by $M + \hat{H}_I/c^2$ in \hat{H}_0 (see Fig. S1(a)). The replacement in the kinetic energy term of \hat{H}_0 can lead to second-order Doppler shift,

$$\hat{H}_{\text{SDS}} = -\frac{\hat{\mathbf{P}}^2}{2M} \frac{\hat{H}_I}{Mc^2}. \quad (\text{S22})$$

The replacement in the gravitational potential energy term of \hat{H}_0 can lead to gravitational redshift,

$$\hat{H}_{\text{GRS}} = \frac{\phi}{c^2} \hat{H}_I. \quad (\text{S23})$$

We have discussed these two types of corrections in the main text, since they are the dominant GR corrections for optical lattice clocks. Here we list their order of magnitudes in Fig. S1(b).

2. \hat{H}_{other} (see Eq. (S10)). Compared to mass-energy equivalence, \hat{H}_{other} only acts on motional degrees of freedom and does not lead to frequency shifts of the clock transition. For comparison, we still list their orders of magnitude in terms of fractional frequency in Fig. S1(b). The first term of \hat{H}_{other} represents the corrections to the kinetic energy in \hat{H}_0 due to relativistic COM motion, which is at the order of fractional frequency 10^{-29} assuming MHz scale of kinetic energy. The rest of the terms are metric geometry corrections to the kinetic energy and potential energy terms in \hat{H}_0 , which is at the order of 10^{-25} for 1 cm spatial separation. It is worth to mention that the term $M\phi^2/c^2$ in metric geometry corrections depends quadratically on the spatial separation ($\sim Z^2$), and this term will become relevant in the case of larger spatial separations such as atom interferometers.
 3. Corrections in \hat{H}_I (see Eq. (S16)). The special relativistic corrections $\hat{H}_{I,\text{SR}}$, as well as the terms related to electron spin, can give rise to atomic fine structure, which has already been taken into account in standard cold atom experiments. As for the metric geometry corrections $\hat{H}_{I,\text{GR}}$, Ref. [S3] points out that $\hat{H}_{I,\text{GR}}$ is off-diagonal in the unperturbed eigenbasis of internal states, so the corrections to the internal energy is negligible. Here, we typically assume \hat{H}_I is the same as the internal Hamiltonian used in standard AMO experiments including atomic fine structure and hyperfine structure. On the other hand, $\hat{H}_{I,\text{GR}}$ might lead to corrections to the internal wave function, so the dipole matrix elements might need to be corrected in \hat{H}_{AL} , although it is suppressed due to the small spatial separation in optical clocks.
- \hat{H}_{AL} describes the couplings to external electromagnetic field, which is relevant for the optical lattice beam as well as the clock laser beam. Although the higher order terms in multipolar expansion can play a more important role compared to the post-Newtonian corrections, here we only focus on the post-Newtonian corrections to the leading order electric dipole terms. Under electric dipole approximation, we have [S2, S8]

$$\hat{H}_{AL} = -\hat{\mathbf{d}} \cdot \mathbf{E} + \frac{1}{2M} \left[\hat{\mathbf{P}} \cdot (\hat{\mathbf{d}} \times \mathbf{B}) + (\hat{\mathbf{d}} \times \mathbf{B}) \cdot \hat{\mathbf{P}} \right], \quad (\text{S24})$$

where $\hat{\mathbf{d}}$ is the electric dipole moment. In Eq. (S24), the first term is the standard electric dipole couplings, and the second term is a relativistic correction term known as the Röntgen term, describing the coupling between a moving dipole and a magnetic field. The Röntgen term is generated by the Lorentz transformation of electric field \mathbf{E} due to relativistic COM motion. We consider monochromatic light field in the following form, $\mathbf{E} = \mathbf{E}^{(+)}e^{-i\omega t} + \text{H.c.}$, $\mathbf{B} = \mathbf{B}^{(+)}e^{-i\omega t} + \text{H.c.}$, where ω is the laser frequency. First we focus on the post-Newtonian corrections to the optical lattice beam:

1. Röntgen term. For simplicity, we assume the lattice AC Stark shifts are dominated by a single dipole-allowed transition $|a\rangle \rightarrow |b\rangle$, so the AC Stark shifts for internal state $|a\rangle$ is given by second-order perturbation theory,

$$\hat{H}_{\text{ac}} \approx -\frac{\langle a|\hat{H}_{AL}|b\rangle\langle b|\hat{H}_{AL}|a\rangle}{E_b - E_a - \hbar\omega_L}, \quad (\text{S25})$$

where ω_L is the frequency of the lattice beam, E_a, E_b are the energy of states $|a\rangle$ and $|b\rangle$ respectively. Here we assume linear polarization of the lattice beam, with $\mathbf{E}^{(+)} = \mathcal{E} \cos(k_L Z)\vec{X}$, $\mathbf{B}^{(+)} = (i\mathcal{E}/c) \sin(k_L Z)\vec{Y}$ and propagation direction \vec{Z} . Here the vector symbol \vec{X} means a unit vector along X direction. Plugging in Eq. (S25), we have

$$\hat{H}_{\text{ac}} \approx -\alpha_{\text{E1}}\mathcal{E}^2 \cos^2(k_L Z) + \alpha_{\text{E1}}\mathcal{E}^2 \frac{\hbar\omega_L}{Mc^2} \sin^2(k_L Z), \quad (\text{S26})$$

where $\alpha_{\text{E1}} = \langle a|\hat{\mathbf{d}} \cdot \vec{X}|b\rangle\langle b|\hat{\mathbf{d}} \cdot \vec{X}|a\rangle/(E_b - E_a - \hbar\omega)$ is the electric dipole polarizability. Here, the first term is the standard optical lattice potential, and the second term is the corrections due to the Röntgen term. This leads to a correction of the lattice depth at the order of $\hbar\omega_L/Mc^2 \sim 10^{-11}$, which is equivalent to a fractional frequency of 10^{-20} for a MHz trapping potential. However, this term does not lead to frequency shifts of the clock transition in a magic wavelength lattice, which means the same α_{E1} for the ground and excited states of the clock transition.

2. Metric geometry corrections to electromagnetic plane waves. As pointed out in Ref. [S4], the calculation of the electromagnetic field is based on solving Maxwell equations under the post-Newtonian metric. For example, the plane wave propagating along \hat{Z} direction (electric field polarized along \hat{X} direction) should be corrected in the following way,

$$\mathbf{E} \propto \left(\left(1 - (\gamma + 1)\frac{\phi}{c^2}\right) \exp \left[-i\omega T \pm \left(1 - \frac{\gamma + 1}{2}\frac{\phi}{c^2}\right) ikZ \right] + \text{c.c.}, 0, 0 \right), \quad (\text{S27})$$

where $k = \omega/c$. As shown in Eq. (S27), we have ϕ/c^2 corrections in the amplitude and phase of the electric field. Note that this term does not lead to differential AC Stark shifts, while it leads to spatial dependent lattice depth and lattice spacing. Such type of correction has negligible effects in optical clocks due to the small spatial separation (fractional frequency 10^{-27} or smaller for 1 cm separation), while it will become relevant in the case of larger spatial separations such as atom interferometers.

We then focus on the post-Newtonian corrections to the clock laser beam. We consider the case of the carrier transition without changing the motional degrees of freedom (motional wave function $\psi_e \approx \psi_g$). Similar to the discussion of the lattice beam, the ϕ/c^2 corrections due to metric geometry are suppressed due to the small spatial separation of the optical clocks. For simplicity, we consider the clock laser beam propagating along \vec{X} direction, with $\mathbf{E}^{(+)} = \mathcal{E}e^{ik_L X}\vec{Z}$, $\mathbf{B}^{(+)} = -(\mathcal{E}/c)e^{ik_L X}\vec{Y}$, the Rabi frequency is given by

$$\Omega_{\text{clk}} = -\frac{\langle e|\hat{\mathbf{d}} \cdot \vec{Z}|g\rangle\mathcal{E}}{\hbar} \left[\int d^3\mathbf{R} \psi_e^* e^{ik_L X} \psi_g - \frac{1}{2Mc} \int d^3\mathbf{R} \psi_e^* (\hat{P}_X e^{ik_L X} + e^{ik_L X} \hat{P}_X) \psi_g \right]. \quad (\text{S28})$$

If we assume the motional states of the atoms are approximately harmonic oscillator states, since $\hat{P}_X e^{ik_L X} + e^{ik_L X} \hat{P}_X$ is off-diagonal in the harmonic oscillator basis, the effects of Röntgen term are significantly suppressed for the carrier transition. On the other hand, \hat{H}_{SDS} due to mass-energy equivalence couples the ground band Wannier function to high bands, which gives perturbative corrections to ψ_e at the order of 10^{-11} . Therefore, the relativistic corrections should be at the order of 10^{-11} for Ω_{clk} , which is equivalent to $10^{-26} - 10^{-25}$ in fractional frequency unit assuming Ω_{clk} in the range of 1 – 10 Hz.

C. Intuitive discussion of post-Newtonian atomic interactions

Here we would like to briefly discuss our intuition for post-Newtonian corrections on atomic interactions. As for the cavity-mediated interactions, post-Newtonian corrections lie in the atom-light couplings and the analysis is similar to the discussion of Ω_{clk} in the previous subsection, thus we can reasonably assume 10^{-11} corrections to the cavity-mediated interactions. As we discuss in the main text, NJ_{\perp} can be of the order of $1 - 10$ Hz for clock transition [S9], so the post-Newtonian corrections are at the order of fractional frequency $10^{-26} - 10^{-25}$, which is negligible for current experiments.

As for the contact interaction, we consider the major source of corrections is the mass-energy equivalence, as we discussed below. Our analysis is based on the s -wave interaction Hamiltonian,

$$\hat{H}_s = \frac{2\pi\hbar^2 a_{eg}^-}{\mu} \int d^3\mathbf{R} \hat{\psi}_e^\dagger(\mathbf{R}) \hat{\psi}_g^\dagger(\mathbf{R}) \hat{\psi}_g(\mathbf{R}) \hat{\psi}_e(\mathbf{R}), \quad (\text{S29})$$

where $\mu = M_e M_g / (M_e + M_g)$ is the reduced mass, and $a_{eg}^- = 69.1a_0$ is the s -wave scattering length [S7, S10]. Here we will simply assume the C_6 coefficient remains unchanged. The effects of mass-energy equivalence on the s -wave interaction are as follows:

- Correction of the s -wave scattering length and the reduced mass. Based on Ref. [S11], the s -wave scattering length can be estimated by

$$a_{eg}^- = \bar{a}_{eg} \left(1 - \tan \left(\Phi - \frac{\pi}{8} \right) \right), \quad \bar{a}_{eg} = \frac{2\pi}{[\Gamma(1/4)]^2} \left(\frac{2\mu C_{6,eg}}{\hbar^2} \right)^{1/4}, \quad (\text{S30})$$

where $\Phi = \int_{r_0}^{\infty} dr \sqrt{2\mu[-V(r)]}/\hbar$ is the WKB phase, with r_0 the classical turning point and $V(r)$ the molecular potential. To remove the $\text{mod}\pi$ ambiguity of Φ , here we note that Φ/π is directly related to the number of bound states N_b in the molecular potential,

$$N_b = \left\lfloor \frac{\Phi}{\pi} - \frac{5}{8} \right\rfloor + 1. \quad (\text{S31})$$

In the formula above, $C_{6,eg} = 3880E_h a_0^6$ is the C_6 coefficient for eg channel of ^{87}Sr atoms [S10], with E_h the Hartree energy and a_0 the Bohr radius, which leads to $\bar{a}_{eg} = 75.4a_0$. Now we apply the mass-energy equivalence, which gives

$$\mu = \frac{M}{2} \left(1 + \frac{\hbar\omega_0}{2Mc^2} \right), \quad (\text{S32})$$

$$\tilde{a}_{eg}^- = a_{eg}^- \left(1 + \frac{\hbar\omega_0}{8Mc^2} \right) \left(1 - 1.099\Phi \frac{\hbar\omega_0}{4Mc^2} \right). \quad (\text{S33})$$

- Correction of the single-atom wave function. Since \hat{H}_{SDS} couples the ground band Wannier function to high bands, we have perturbative corrections to the ground band Wannier function of $|e\rangle$ state. If we approximate the Wannier functions as the harmonic oscillator states, we get

$$\psi_g(X) \approx \psi_0(X), \quad \psi_e(X) \approx \psi_0(X) - \frac{\sqrt{2}\hbar\omega_0}{8Mc^2} \psi_2(X), \quad (\text{S34})$$

where ψ_n is the wave function of harmonic oscillator level n . The same formula can apply to Y and Z direction.

Combining all the corrections in Eq. (S32-S34), we can estimate the on-site interaction U by

$$U = \frac{2\pi\hbar^2 \tilde{a}_{eg}^-}{\mu} \int dX [\psi_e(X)]^2 [\psi_g(X)]^2 \int dY [\psi_e(Y)]^2 [\psi_g(Y)]^2 \int dZ [\psi_e(Z)]^2 [\psi_g(Z)]^2 \quad (\text{S35})$$

$$\approx U_0 \left(1 - 1.099\Phi \frac{\hbar\omega_0}{4Mc^2} \right),$$

where $U_0 = \sqrt{8/\pi} (k_L a_{eg}^-) (E_R V_X V_Y V_Z)^{1/4}$. This calculation shows that the main contribution comes from the WKB phase. Up to date there are no experimental measurements for the number of bound states in the eg channel of ^{87}Sr atoms. If we assume Φ/π falls into the range of $10^1 - 10^2$, this leads to $10^{-10} - 10^{-9}$ corrections to U , which is equivalent to fractional frequency $10^{-22} - 10^{-21}$ for U at kHz scale. We note that this correction is much smaller than the modification of bare scattering length due to the lattice potential itself [S12, S13], and therefore can be ignored for current experiments.

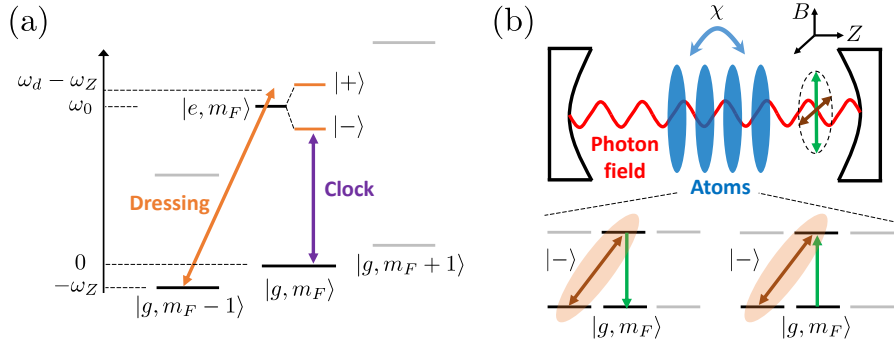


Fig. S2. (a) Schematic of the dressing protocol. We apply dressing laser connecting $|e, m_F\rangle$ with $|g, m_F - 1\rangle$ states, which leads to the dressed basis $|+\rangle$ and $|-\rangle$. We then define the new clock qubit based on the transition between $|g, m_F\rangle$ and $|-\rangle$ states. (b) Schematic of the cavity-mediated interactions in the dressed basis. The cavity axis is along Z and the quantization axis is along magnetic field B labeled in the plot. The additional nuclear spin state in the dressing protocol allows for coupling to two polarization modes in the cavity and enhancing the tunability of the cavity-mediated interactions.

S2. DRESSING PROTOCOL

A. Derivation

In Fig. 2 of the main text, we discussed state dressing protocol proposed to tune and distinguish the mass-energy equivalence from other effects. We explain the protocol in more detail. We consider three internal levels $|e, m_F\rangle$, $|g, m_F\rangle$ and $|g, m_F - 1\rangle$. A dressing laser (with Rabi frequency Ω , laser frequency ω_d) is used to couple $|e, m_F\rangle$ with $|g, m_F - 1\rangle$ states (see Fig. S2(a)). Due to magnetic Zeeman shifts, the clock transitions between different nuclear spins are frequency resolved, thus we assume the modification on other states are typically small. In the rotating frame of the dressing laser, the Hamiltonian of internal levels plus dressing laser becomes

$$\hat{H}_{I+D} = \hbar\omega_0|e, m_F\rangle + \hbar(\omega_0 + \delta)|g, m_F - 1\rangle + \frac{\hbar\Omega}{2}(|e, m_F\rangle\langle g, m_F - 1| + \text{H.c.}), \quad (\text{S36})$$

where $\delta = \omega_d - \omega_0 - \omega_Z$ is the detuning of the dressing laser, and ω_Z the Zeeman shift between $|g, m_F\rangle$ and $|g, m_F - 1\rangle$ states. We set the energy of $|g, m_F\rangle$ state to 0. The eigenstates of this Hamiltonian are given by

$$|+\rangle = C_1|e, m_F\rangle + C_2|g, m_F - 1\rangle, \quad E_+/\hbar = \omega_0 + \frac{\delta}{2} + \frac{1}{2}\sqrt{\Omega^2 + \delta^2}, \quad (\text{S37})$$

$$|-\rangle = -C_2|e, m_F\rangle + C_1|g, m_F - 1\rangle, \quad E_-/\hbar = \omega_0 + \frac{\delta}{2} - \frac{1}{2}\sqrt{\Omega^2 + \delta^2}, \quad (\text{S38})$$

where

$$C_1 = \frac{1}{\sqrt{2}} \left(1 - \frac{\delta}{\sqrt{\Omega^2 + \delta^2}} \right)^{1/2}, \quad C_2 = \frac{1}{\sqrt{2}} \left(1 + \frac{\delta}{\sqrt{\Omega^2 + \delta^2}} \right)^{1/2}. \quad (\text{S39})$$

Since $\omega_Z \ll \omega_0$, we can ignore the mass difference between $|g, m_F\rangle$ and $|g, m_F - 1\rangle$ states. The corrections from the second order Doppler shift \hat{H}_{SDS} and gravitational redshift \hat{H}_{GRS} take the following form,

$$\hat{H}_{\text{SDS}} = -\hbar\omega_0 \frac{\hat{\mathbf{P}}^2}{2M^2c^2} |e\rangle\langle e|, \quad \hat{H}_{\text{GRS}} = \hbar\omega_0 \frac{gZ}{c^2} |e\rangle\langle e|. \quad (\text{S40})$$

Since \hat{H}_{SDS} and \hat{H}_{GRS} are much smaller than the energy gap $\sqrt{\Omega^2 + \delta^2}$, we can restrict the dynamics within the effective two level system formed by $|g, m_F\rangle$ and $|-\rangle$ states if tuning the clock laser frequency resonant with this transition. In this case we define the projection operator

$$\hat{\mathcal{P}} = |-\rangle\langle -| + |g, m_F\rangle\langle g, m_F|. \quad (\text{S41})$$

Using the projection operator, \hat{H}_{SDS} and \hat{H}_{GRS} become

$$\hat{\mathcal{P}}\hat{H}_{\text{SDS}}\hat{\mathcal{P}} = -\hbar\omega_0\frac{\hat{\mathbf{P}}^2}{2M^2c^2}|C_2|^2|-\rangle\langle-|, \quad \hat{\mathcal{P}}\hat{H}_{\text{GRS}}\hat{\mathcal{P}} = \hbar\omega_0\frac{gZ}{c^2}|C_2|^2|-\rangle\langle-|, \quad (\text{S42})$$

which is equivalent to a modification of the mass defect,

$$\Delta M = |C_2|^2\Delta M_0, \quad (\text{S43})$$

where $\Delta M_0 = \hbar\omega_0/c^2$ is the mass defect without the dressing protocol. The GRS leads to a position-dependent correction of the dressed state energy E_- (we do not include the second order Doppler shift for simplicity),

$$E_-(Z) = E_- + \frac{\hbar\omega_0g}{c^2}|C_2|^2Z, \quad (\text{S44})$$

which can be resolved via clock spectroscopy in the effective two level system formed by $|g, m_F\rangle$ and $|-\rangle$ states.

All the discussion above is in the rotating frame of the dressing laser. When an atom is in the state $|-\rangle$, the probability to populate the excited clock state is $|C_2|^2$ and therefore in the lab frame it has an average energy $\approx |C_2|^2\hbar\omega_0$. This is another way to understand how the dressing laser enables the tunability of the mass defect ΔM .

B. Technical considerations

Due to experimental imperfection, spatial inhomogeneities exist for the atomic frequency and the parameters δ and Ω in E_- . The effects of the GRS will be washed out if the inhomogeneities are much larger than the redshift value. For 1 cm spatial separation, the GRS is at the order of mHz, thus one needs to control the inhomogeneities below 10^{-4} Hz for direct observation of the GRS.

Relating the single atom energies, the leading order contributions are from position-dependent Zeeman shifts due to spatial inhomogeneities in the magnetic field. One can suppress first order Zeeman shifts by probing opposite nuclear spin states and calculating the averaged frequency, which has been already demonstrated in Ref. [S6]. The same idea also works for the dressing protocol. One can average the transition frequency of $|g, m_F\rangle \leftrightarrow (-C_2|e, m_F\rangle + C_1|g, m_F - 1\rangle)$ and $|g, -m_F\rangle \leftrightarrow (-C_2|e, -m_F\rangle + C_1|g, -m_F + 1\rangle)$. Without shot-to-shot fluctuations, this approach allows for exact cancellation of the effects from magnetic field gradients.

Since the GRS behaves like a magnetic field gradient across the atomic sample in the case of two-level systems, it is important to distinguish it from any residual magnetic field gradient. Suppose there is no gravitational redshift in the system, and there is a small magnetic field gradient term adding on top of a constant magnetic field, then we have $\omega_0(Z) = \omega_0 + (\eta_e - \eta_g)m_FZ$, $\omega_Z(Z) = \omega_Z + \eta_gZ$, where $\eta_e = -\mathcal{G}_{^3P_0}\mu_B\partial_Z B$, $\eta_g = -\mathcal{G}_{^1S_0}\mu_B\partial_Z B$, with $\mathcal{G}_{^3P_0}$ and $\mathcal{G}_{^1S_0}$ representing the Landé g-factors, and μ_B is the Bohr magneton. So the first-order perturbation correction of the energy of the $|-\rangle$ state is given by

$$E_-(Z) = E_- + \left[|C_2|^2(\eta_e - \eta_g)m_F - |C_1|^2\eta_g \right] Z. \quad (\text{S45})$$

Since $\eta_g \neq 0$, we find different dependence by varying δ compared to the gravitational redshift (see Eq. (S44)). The reason is that different ground-state nuclear spins have the same mass but different Zeeman shifts.

As for the dressing laser Rabi frequency Ω , the leading order contributions are from the spatial profile of the laser beam. If we denote the modification of Ω as $\Delta\Omega$, the change of E_- is given by

$$\Delta E_-/\hbar = -\frac{1}{2}\sqrt{\Omega^2 + \delta^2} \left(1 + \frac{(\Delta\Omega)\Omega}{\Omega^2 + \delta^2} \right). \quad (\text{S46})$$

For ^{87}Sr atoms, the Zeeman shifts between nuclear spin states are at the order of 10^2 Hz, in order to frequency resolve a single transition between nuclear spin states, we have $\Omega/2\pi \sim 10$ Hz. So the requirement $\Delta\Omega/2\pi < 10^{-4}$ Hz is equivalent to $\Delta\Omega/\Omega < 10^{-5}$. In principle, this requirement is achievable using an ultrastable cavity, which allows for precise control of the spatial mode of the dressing laser. An alternative approach is to reduce this requirement is to notice that the change of E_+ due to $\Delta\Omega$ as the opposite sign,

$$\Delta E_+/\hbar = \frac{1}{2}\sqrt{\Omega^2 + \delta^2} \left(1 + \frac{(\Delta\Omega)\Omega}{\Omega^2 + \delta^2} \right). \quad (\text{S47})$$

If we average the transition frequency of $|g, m_F\rangle \leftrightarrow |- \rangle$ and $|g, m_F\rangle \leftrightarrow |+ \rangle$, we get

$$\frac{E_-(Z) + E_+(Z)}{2} = \hbar\omega_0 + \frac{\hbar\delta}{2} + \frac{1}{2} \frac{\hbar\omega_0 g}{c^2} Z. \quad (\text{S48})$$

In this way, the averaged transition frequency becomes independent of Ω . Even though one sacrifices the full tunability of gravitational redshift, it is still changed to half of its value without dressing.

C. Contact interactions

Here we analyze the effects of the dressing protocol on the interatomic s -wave interactions. We start from the following second quantized Hamiltonian describing the s -wave interaction of alkaline earth atoms due to $SU(n)$ symmetry [S7],

$$\begin{aligned} \hat{H}_s = & \frac{2\pi\hbar^2 a_{gg}}{M} \sum_{\substack{mm' \\ (m \neq m')}} \int d^3\mathbf{R} \hat{\psi}_{gm}^\dagger(\mathbf{R}) \hat{\psi}_{gm'}^\dagger(\mathbf{R}) \hat{\psi}_{gm'}(\mathbf{R}) \hat{\psi}_{gm}(\mathbf{R}) \\ & + \frac{2\pi\hbar^2 a_{ee}}{M} \sum_{\substack{mm' \\ (m \neq m')}} \int d^3\mathbf{R} \hat{\psi}_{em}^\dagger(\mathbf{R}) \hat{\psi}_{em'}^\dagger(\mathbf{R}) \hat{\psi}_{em'}(\mathbf{R}) \hat{\psi}_{em}(\mathbf{R}) \\ & + \frac{2\pi\hbar^2 (a_{eg}^- + a_{eg}^+)}{M} \sum_{mm'} \int d^3\mathbf{R} \hat{\psi}_{gm}^\dagger(\mathbf{R}) \hat{\psi}_{em'}^\dagger(\mathbf{R}) \hat{\psi}_{em'}(\mathbf{R}) \hat{\psi}_{gm}(\mathbf{R}) \\ & + \frac{2\pi\hbar^2 (a_{eg}^- - a_{eg}^+)}{M} \sum_{mm'} \int d^3\mathbf{R} \hat{\psi}_{gm}^\dagger(\mathbf{R}) \hat{\psi}_{em'}^\dagger(\mathbf{R}) \hat{\psi}_{em}(\mathbf{R}) \hat{\psi}_{gm'}(\mathbf{R}). \end{aligned} \quad (\text{S49})$$

Here m is the label of nuclear spins $-F, -F+1, \dots, F$, and a_{gg}, a_{ee}, a_{eg}^- and a_{eg}^+ are the s -wave scattering lengths.

Assuming the frequency difference between nuclear spins (Zeeman shifts) and energy gap $\sqrt{\Omega^2 + \delta^2}$ between two dressed states are typically larger than the interaction strength, one can restrict the dynamics within two levels, $|\downarrow\rangle \equiv |g, m_F\rangle$ and $|\uparrow\rangle \equiv |- \rangle$. Projecting the interaction Hamiltonian into these two states (see Eq. (S41)), we have

$$\hat{\mathcal{P}} \hat{H}_s \hat{\mathcal{P}} = \frac{4\pi\hbar^2}{M} \left(|C_1|^2 a_{gg} + |C_2|^2 a_{eg}^- \right) \int d^3\mathbf{R} \hat{\psi}_\uparrow^\dagger(\mathbf{R}) \hat{\psi}_\downarrow^\dagger(\mathbf{R}) \hat{\psi}_\downarrow(\mathbf{R}) \hat{\psi}_\uparrow(\mathbf{R}). \quad (\text{S50})$$

In this way, we modify the on-site interaction strength U by

$$\frac{U}{U_0} = \frac{|C_1|^2 a_{gg} + |C_2|^2 a_{eg}^-}{a_{eg}^-}. \quad (\text{S51})$$

D. Cavity-mediated interactions

Here we analyze the effects of the dressing protocol on the cavity-mediated interactions. Refs. [S14, S15] provide a detailed discussion of cavity-mediated interactions for multilevel alkaline earth atoms. Here we focus on the case that the quantization axis for nuclear spins is perpendicular to the cavity axis (see Fig. S2(b)). In this case, the two polarization modes supported by the cavity can drive the π transition and the linear combination of σ^+ and σ^- transitions, so we can define the multilevel raising operators for these two polarization modes,

$$\hat{\Pi}^+ = \sum_{jm} C_m^0 |e_m\rangle_j \langle g_m|, \quad \hat{\Sigma}^+ = \sum_{jm} \frac{i}{\sqrt{2}} (C_m^{-1} |e_{m-1}\rangle_j \langle g_m| + C_m^{+1} |e_{m+1}\rangle_j \langle g_m|), \quad (\text{S52})$$

where j is the label of atoms, m is the label of nuclear spins, and $C_m^\sigma \equiv \langle F, m; 1, \sigma | F, m + \sigma \rangle$ are the Clebsch-Gordan coefficients. Based on Ref. [S14], the multilevel exchange interactions take the following form,

$$\hat{H}_c / \hbar = \chi (\hat{\Pi}^+ \hat{\Pi}^- + \hat{\Sigma}^+ \hat{\Sigma}^-), \quad (\text{S53})$$

with $\hat{\Pi}^- = (\hat{\Pi}^+)^\dagger$ and $\hat{\Sigma}^- = (\hat{\Sigma}^+)^\dagger$.

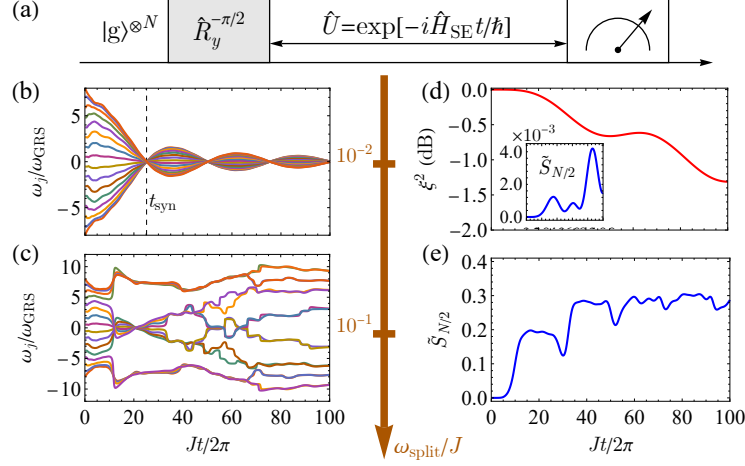


Fig. S3. (a) We prepare a product state with all atoms in $|g\rangle$ state and apply a laser pulse $\hat{R}_y^{-\pi/2} = \exp(i\frac{\pi}{2}\hat{S}^y)$ to start the dynamics. We focus on a single tube with $N = 16$ atoms evolving under the Hamiltonian \hat{H}_{SE} (Eq. (S56)), and then perform measurements for each atom. (b) Individual atomic frequency shift ω_j with $\omega_{\text{split}}/NJ_{\perp} = 10^{-2}$. Synchronization of atomic frequencies can be reached at time t_{syn} . (c) Individual atomic frequency shift ω_j with $\omega_{\text{split}}/NJ_{\perp} = 10^{-1}$. Global synchronization fails to occur in this regime. (d) Spin squeezing parameter ξ^2 and normalized Rényi entropy $\tilde{S}_{N/2}$ in the case of (b). (e) Normalized Rényi entropy $\tilde{S}_{N/2}$ in the case of (c). The interplay between cavity-mediated interactions and gravitational redshift can lead to entanglement generation for both cases.

Assuming the frequency difference between nuclear spins (Zeeman shifts) and energy gap $\sqrt{\Omega^2 + \delta^2}$ between two dressed states are typically larger than the interaction strength χN , one can restrict the dynamics within two levels, $|\downarrow\rangle \equiv |g, m_F\rangle$ and $|\uparrow\rangle \equiv |-\rangle$. In this two-level system, one can define collective spin operators, $\hat{S}^+ = \sum_j |\uparrow\rangle_j \langle\downarrow|$, $\hat{S}^- = (\hat{S}^+)^\dagger$, and $\hat{S}^z = \sum_j (|\uparrow\rangle_j \langle\uparrow| - |\downarrow\rangle_j \langle\downarrow|)/2$. Projecting \hat{H}_c into this two-level system (see Eq. (S41)), we get

$$\hat{\mathcal{P}}\hat{H}_c\hat{\mathcal{P}} = \chi(C_{m_F}^0)^2|C_2|^2\hat{S}^+\hat{S}^- + \chi\frac{(C_{m_F-1}^{+1})^2}{2}|C_1|^2|C_2|^2\left(\frac{N}{2} + \hat{S}^z\right)^2. \quad (\text{S54})$$

In this way, we modify J_{\perp} and J_z by

$$J_{\perp} = \chi(C_{m_F}^0)^2|C_2|^2, \quad J_z = \chi\frac{(C_{m_F-1}^{+1})^2}{2}|C_1|^2|C_2|^2. \quad (\text{S55})$$

S3. ADDITIONAL NUMERICAL RESULTS

In the main text, we have shown that frequency synchronization and entanglement generation can be achieved due to the interplay between cavity-mediated interactions and gravitational redshift. Here we show that similar phenomena can be achieved if we replace cavity-mediated interactions by superexchange interactions. For simplicity, we consider the case $V_Z \ll V_X = V_Y$ for a 3D lattice with ^{87}Sr atoms in the ground band, so the system behaves as an array of independent tubes along the gravitational potential (Z axis). We assume the system is in the Mott insulator regime with one atom per lattice site, where the leading dynamics can be described by superexchange interactions mediated by motion between nearest neighbor sites [S16]. The Hamiltonian within a tube can be written in terms of spin-1/2 operators $\hat{s}_j^{x,y,z} = \hat{c}_{j\beta}^\dagger \sigma_{\beta\beta'}^{x,y,z} \hat{c}_{j\beta'}$ in the two-level system defined by the dressing scheme, where $\sigma^{x,y,z}$ are Pauli matrices, $\hat{c}_{j\beta}$ is the fermionic annihilation operator for lattice site index j and spin label $\beta = \{\uparrow, \downarrow\}$. We get

$$\hat{H}_{SE}/\hbar = J \sum_j \hat{\mathbf{s}}_j \cdot \hat{\mathbf{s}}_{j+1} + \omega_{GRS} \sum_j j \hat{s}_j^z, \quad (\text{S56})$$

where $\hbar\omega_{GRS} = (\Delta M)ga_L$ is the gravitational redshift between nearest neighbor sites, and $\hbar J = 4\tau^2/U_{\text{eff}}$ is the superexchange interaction strength. Here $U_{\text{eff}} = (U^2 - (Mga_L)^2)/U$, with U the on-site interaction strength. Based on Eq. (S56), a magnetic field gradient will in principle give rise to similar single-atom inhomogeneities in the Hamiltonian.

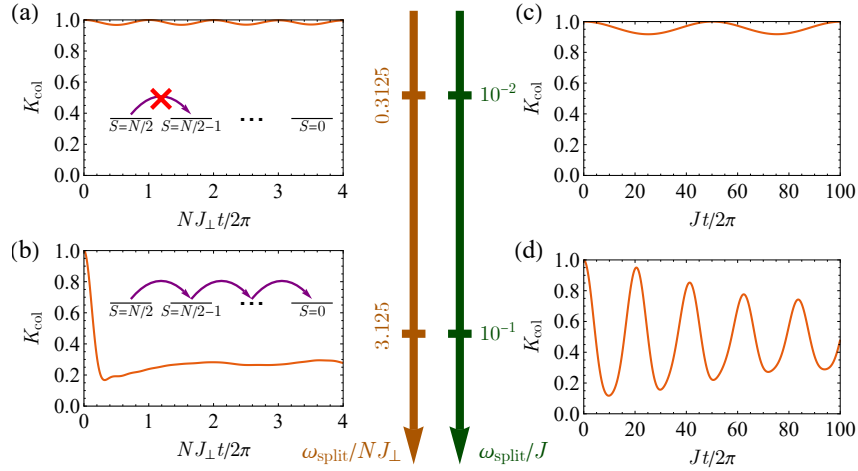


Fig. S4. We evolve the system based on the time sequence in Fig. 3 in the main text and calculate the expectation value $K_{\text{col}} = \langle \hat{\mathbf{S}} \cdot \hat{\mathbf{S}} \rangle / [\frac{N}{2}(\frac{N}{2} + 1)]$ as a function of evolution time. (a,b) We consider Hamiltonian of cavity-mediated interactions \hat{H}_{cav} with $J_{\perp} = J_z$ (Eq. (5) in the main text). The choice of parameters is the same as Fig. S3. (c,d) We consider Hamiltonian of nearest-neighbor superexchange interaction \hat{H}_{SE} (Eq. (S56)). The choice of parameters is the same as Fig. 3 in the main text.

The combination of the dressed states allows us to tune the value of U by coupling to different atomic collision channels (see previous sections). This assumes all the interaction strengths are smaller than dressed state energy gap $\sqrt{\Omega^2 + \delta^2}$ and Zeeman shifts between nuclear spins, to restrict dynamics within two levels. Note that mass-energy equivalence might also lead to corrections of U via modifying scattering lengths (see previous sections), while they are smaller than the current uncertainty of interaction parameters [S12].

In Fig. S3, we perform the same analysis as Fig. 3 in the main text, while replacing cavity-mediated interactions \hat{H}_{cav} (Eq. (5) in the main text) by the nearest-neighbor superexchange interaction \hat{H}_{SE} (see Eq. (S56)). Since the initial state is an eigenstate of the interaction terms, and the interplay between interaction and gravitational redshift can lead to quantum dynamics away from this eigenstate and generate quantum entanglement, similar to the phenomena discussed in Fig. 3 in the main text. In the interaction dominant regime, we find frequency synchronization and spin squeezing generation due to many-body gap protection. While in the regime where the interaction strength is comparable with the gravitational redshift, frequency synchronization fails to occur, and we find a faster growth of normalized Rényi entropy.

In contrast to the cavity-mediated interactions discussed in the main text, the spin wave analysis (see the next section) of superexchange interaction shows a scaling of $\Delta E \propto J/N^2$ for the many-body gap and $Jt_{\text{syn}} \propto N^2$ for the synchronization time. For the typical OLC setup [S16], the frequency synchronization can be reached within 1 s for a tube with $N = 16$. Considering the 3D lattice with an array of independent tubes, the total atom number would be $16^3 = 4096$, which is at the same order of magnitude as the atom number in Ref. [S16].

In Fig. S4, we use the same time sequence as Fig. 3 in the main text, and calculate the expectation value $\langle \hat{\mathbf{S}} \cdot \hat{\mathbf{S}} \rangle$ as a function of the evolution time. Note that in a given total spin- S manifold, we have $\langle \hat{\mathbf{S}} \cdot \hat{\mathbf{S}} \rangle = S(S+1)$. So $\langle \hat{\mathbf{S}} \cdot \hat{\mathbf{S}} \rangle$ can serve as a measure of population in the collective manifold ($S = N/2$), spin-wave manifold ($S = N/2 - 1$), as well as the manifolds with lower total spin. We consider both nearest-neighbor superexchange interaction \hat{H}_{SE} (Eq. (S56)) and cavity-mediated interaction \hat{H}_{cav} with $J_{\perp} = J_z$ (Eq. (5) in the main text). In the interaction dominant regime where frequency synchronization can occur, we find undamped oscillations between the collective manifold ($S = N/2$) and the spin-wave manifold ($S = N/2 - 1$). In the other regime where frequency synchronization fails to occur, the system can evolve to manifolds with lower total spin.

S4. ANALYTIC RESULTS FOR FREQUENCY SYNCHRONIZATION

In the main text, we discuss the interplay between atomic interactions (contact interaction or cavity mediated interactions) and gravitational redshift. Here we would like to provide analytic spin-wave calculations based on two different approaches, including Holstein–Primakoff approximation and restriction of dynamics within collective and spin-wave manifold. We focus on the single chain of N atoms and consider each atom as a spin-1/2 particle with operators $\hat{s}_n^{x,y,z}$, and in this case we also use N to label the number of lattice sites. Based on our protocol in Fig. 3

and Fig. 4 in the main text, the frequency of each atom $\omega_n(t)$ can be estimated by

$$\omega_n(t) = \frac{1}{t} \arctan \left(\frac{\langle \hat{s}_n^y(t) \rangle}{\langle \hat{s}_n^x(t) \rangle} \right). \quad (\text{S57})$$

The rigorous definition of the synchronization time t_{syn} is the time for the first minimum in the variance of atomic frequencies. In fact, we can approximately reach the zero crossing of $\omega_n(t)$ for all the n at t_{syn} , as demonstrated by the analytic results below and by numerical evidences.

A. Holstein–Primakoff approximation

We would like to use Holstein–Primakoff approximation to describe the case with an unentangled initial state (see Fig. 3 in the main text). Considering the initial state with all N spins pointing to $+x$ direction, we can approximate the spin-1/2 operators as

$$\hat{s}_n^x = \frac{1}{2} - \hat{a}_n^\dagger \hat{a}_n, \quad \hat{s}_n^y \approx \frac{\hat{a}_n + \hat{a}_n^\dagger}{2}, \quad \hat{s}_n^z \approx \frac{\hat{a}_n - \hat{a}_n^\dagger}{2i}. \quad (\text{S58})$$

In this way, the initial state becomes the vacuum state of all these bosonic operators. In the following, we will plug these bosonic operators into the Hamiltonian and keep the terms up to quadratic order of bosonic operators. We then apply Fourier transform to obtain the bosonic operators for spin waves $k = 2\pi m/N$ with $m = 0, 1, 2, \dots, N-1$,

$$\hat{a}_n = \frac{1}{\sqrt{N}} \sum_k e^{ikn} \hat{a}_k, \quad \hat{a}_n^\dagger = \frac{1}{\sqrt{N}} \sum_k e^{-ikn} \hat{a}_k^\dagger, \quad (\text{S59})$$

and rewrite the Hamiltonian accordingly. The validity of Holstein–Primakoff approximation requires $\langle \hat{a}_n \rangle \ll 1$ for all n . If we define η as the ratio between the maximum redshift in the array ($\omega_{\text{split}} = (N-1)\omega_{\text{GRS}}$) and the smallest spin wave excitation gap (discussed below), the typical condition for validity would be $\eta \ll 1$. In this regime, the frequency of each atom $\omega_n(t)$ can be approximated as

$$\omega_n(t) \approx \frac{2\langle \hat{s}_n^y(t) \rangle}{t}. \quad (\text{S60})$$

1. Nearest-neighbor Heisenberg interactions

Here we consider the Hamiltonian for nearest-neighbor Heisenberg interactions,

$$\hat{H}_1/\hbar = J \sum_{n=0}^{N-2} \hat{\mathbf{s}}_n \cdot \hat{\mathbf{s}}_{n+1} + \omega_{\text{GRS}} \sum_{n=0}^{N-1} \left(n - \frac{N-1}{2} \right) \hat{s}_n^z, \quad (\text{S61})$$

in which we set the average value of gravitational redshift to 0, based on our convention. Applying the Holstein–Primakoff bosons and keeping the terms up to quadratic order, the Hamiltonian in terms of the spin-wave operators becomes

$$\hat{H}_1/\hbar \approx -J \sum_{k \neq 0} \left(1 - \cos(k) \right) \hat{a}_k^\dagger \hat{a}_k + \frac{\omega_{\text{GRS}}}{2i} \sqrt{N} \sum_{k \neq 0} \left(\frac{1}{e^{ik} - 1} \hat{a}_k - \frac{1}{e^{-ik} - 1} \hat{a}_k^\dagger \right). \quad (\text{S62})$$

For simplicity, we ignore the boundary effect in the formula above. Solving the Heisenberg equation of motion for \hat{a}_k with $k \neq 0$, one can finally reach

$$\omega_n(t) \approx -\frac{\omega_{\text{GRS}}}{2} \sum_{k \neq 0} \frac{\sin \left(J(1 - \cos(k))t \right) \sin \left(kn + k/2 \right)}{J(1 - \cos(k))t \sin(k/2)}. \quad (\text{S63})$$

In the limit of $t \rightarrow 0$, we have

$$\omega_n(0) = -\frac{\omega_{\text{GRS}}}{2} \sum_{k \neq 0} \frac{\sin(kn + k/2)}{\sin(k/2)} = -\frac{\omega_{\text{GRS}}}{2} \sum_{k \neq 0} \left(1 + 2 \sum_{j=1}^n \cos(jk) \right) = \omega_{\text{GRS}} \left(n - \frac{N-1}{2} \right), \quad (\text{S64})$$

which agrees with the gravitational redshift value without interactions.

Since the energy gap of spin wave excitation has the smallest value at $k = 2\pi/N$ and $k = 2\pi(N-1)/N$, so the system dynamics is dominated by these two spin wave modes. Therefore, one can conclude that the frequency synchronization occurs at $J(1 - \cos(2\pi/N))t \approx Jt/2(2\pi/N)^2 = \pi$ which gives

$$Jt_{\text{syn}} \approx \frac{N^2}{2\pi}. \quad (\text{S65})$$

In fact, the Jt_{syn} we found numerically is larger by nearly a factor of 4 compared to what we predicted here, since the boundary effect we ignored in the analytic calculation is equivalent to a reduction of spin wave gap. Nevertheless, we are able to capture the N -scaling of t_{syn} (see Fig. S5(a) for numerical calculations). To ensure the validity of the Holstein–Primakoff approximation, we have

$$\eta \sim \frac{\omega_{\text{GRS}}}{J} N^3 \ll 1, \quad (\text{S66})$$

which in principle sets a limit for the largest possible system size.

Within the Holstein–Primakoff approximation, the deviation of $\omega_n(t_{\text{syn}})$ from 0 originates from the non-vanishing contribution of other spin wave modes. Based on Eq. (S63), we can estimate $\sin(J(1 - \cos(k))t_{\text{syn}})/(J(1 - \cos(k))t_{\text{syn}}) \sim O(N^{-2})$, which gives

$$\frac{\omega_n(t_{\text{syn}})}{\omega_n(0)} \sim O\left(\frac{1}{N^2}\right). \quad (\text{S67})$$

2. Collective Heisenberg interactions

Here we consider the Hamiltonian for collective Heisenberg interactions,

$$\hat{H}_2/\hbar = J_{\perp} \sum_{n=0}^{N-1} \sum_{m=0}^{N-1} \hat{\mathbf{s}}_n \cdot \hat{\mathbf{s}}_m + \omega_{\text{GRS}} \sum_{n=0}^{N-1} \left(n - \frac{N-1}{2}\right) \hat{s}_n^z. \quad (\text{S68})$$

Applying the Holstein–Primakoff bosons and keeping the terms up to quadratic order, the Hamiltonian in terms of spin wave operators becomes

$$\hat{H}_2/\hbar \approx -NJ_{\perp} \sum_{k \neq 0} \hat{a}_k^{\dagger} \hat{a}_k + \frac{\omega_{\text{GRS}}}{2i} \sqrt{N} \sum_{k \neq 0} \left(\frac{1}{e^{ik} - 1} \hat{a}_k - \frac{1}{e^{-ik} - 1} \hat{a}_k^{\dagger} \right). \quad (\text{S69})$$

Solving the Heisenberg equation of motion for \hat{a}_k with $k \neq 0$, one can finally reach

$$\omega_n(t) \approx -\frac{\omega_{\text{GRS}}}{2} \frac{\sin(NJ_{\perp}t)}{NJ_{\perp}t} \sum_{k \neq 0} \frac{\sin(kn + k/2)}{\sin(k/2)} = \omega_{\text{GRS}} \frac{\sin(NJ_{\perp}t)}{NJ_{\perp}t} \left(n - \frac{N-1}{2}\right). \quad (\text{S70})$$

Similarly, $\omega_n(0)$ agrees with the gravitational redshift value without interactions. As for the frequency synchronization, it happens at $NJ_{\perp}t = \pi$, which gives

$$J_{\perp}t_{\text{syn}} = \frac{\pi}{N}. \quad (\text{S71})$$

This analytic result agrees with the numerical simulations (see Fig. S5(b)). To ensure the validity of the Holstein–Primakoff approximation, we have

$$\eta \sim \frac{\omega_{\text{GRS}}}{J_{\perp}} \ll 1, \quad (\text{S72})$$

which is independent of the system size. Within the Holstein–Primakoff approximation, there is no deviation of $\omega_n(t_{\text{syn}})$ from 0.

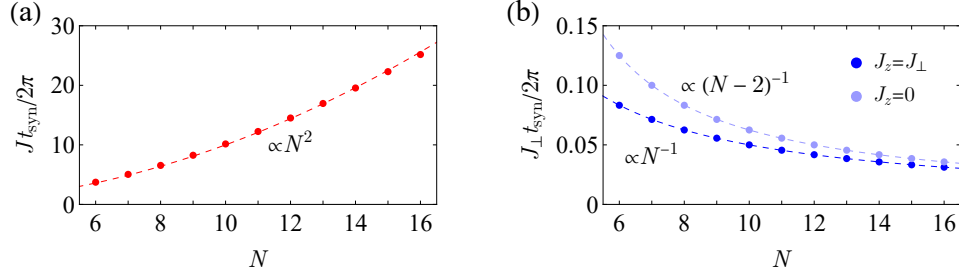


Fig. S5. Scaling of synchronization time t_{syn} as a function of atom number N for (a) contact interactions and (b) cavity-mediated interactions. In (b), we compare the t_{syn} between collective Heisenberg interactions ($J_z = J_\perp$) and spin exchange interactions ($J_z = 0$). All the calculations are based on an initial unentangled state with all the spins pointing to $+x$ direction. See the protocol in Fig. 3(a) in the main text.

B. Restriction within collective and spin-wave manifold for two large spins

For the case with an entangled initial state, it is not possible to use the Holstein–Primakoff approximation. Alternatively, we would like to simplify the Hamiltonian into two large spins ($S_1 = S_2 = N/4$) with effective Heisenberg interaction strength J_{eff} and effective redshift value ω_{eff} ,

$$\hat{H}_{\text{eff}}/\hbar = 2J_{\text{eff}}\hat{\mathbf{S}}_1 \cdot \hat{\mathbf{S}}_2 + \frac{\omega_{\text{eff}}}{2}(\hat{S}_1^z - \hat{S}_2^z). \quad (\text{S73})$$

In the regime $\omega_{\text{eff}} \ll NJ_{\text{eff}}$, we can restrict the dynamics within the collective manifold with total spin $S = N/2$ as well as the spin-wave manifold with total spin $S = N/2 - 1$. Based on the Clebsch-Gordan coefficients, the states in the collective manifold ($S = N/2$) can be expressed as

$$|N/2, m\rangle = \sum_{m_1} \sqrt{\frac{\binom{N/2}{N/4+m_1}\binom{N/2}{N/4+m-m_1}}{\binom{N}{N/2+m}}} |N/4, m_1\rangle_1 |N/4, m-m_1\rangle_2, \quad (\text{S74})$$

and the states in the spin-wave manifold ($S = N/2 - 1$) can be expressed as

$$|N/2 - 1, m\rangle = \sum_{m_1} (2m_1 - m) \sqrt{\frac{\binom{N/2}{N/4+m_1}\binom{N/2}{N/4+m-m_1}}{N\binom{N-2}{N/2-1+m}}} |N/4, m_1\rangle_1 |N/4, m-m_1\rangle_2, \quad (\text{S75})$$

where $\binom{n}{k}$ are binomial coefficients. A key observation from Eq. (S74) and Eq. (S75) is that

$$(\hat{S}_1^z - \hat{S}_2^z)|N/2, m\rangle = \sqrt{\frac{(N/2+m)(N/2-m)}{N-1}} |N/2 - 1, m\rangle. \quad (\text{S76})$$

If we restrict the dynamics within the collective and spin-wave manifold, \hat{H}_{eff} can be reduced to 2×2 matrices in each m sector in the basis $\{|N/2, m\rangle, |N/2 - 1, m\rangle\}$,

$$\hat{H}_{\text{eff},m}/\hbar = \begin{pmatrix} NJ_{\text{eff}} & \frac{\omega_{\text{eff}}}{2} \sqrt{\frac{(N/2+m)(N/2-m)}{N-1}} \\ \frac{\omega_{\text{eff}}}{2} \sqrt{\frac{(N/2+m)(N/2-m)}{N-1}} & 0 \end{pmatrix}. \quad (\text{S77})$$

Also based on Eq. (S74) and Eq. (S75), we have ($j = 1, 2$)

$$\hat{S}_j^+ |N/2, m\rangle = \frac{1}{2} \sqrt{(N/2+m+1)(N/2-m)} |N/2, m+1\rangle - \frac{(-1)^j}{2} \sqrt{\frac{(N/2-m)(N/2-m-1)}{N-1}} |N/2-1, m+1\rangle, \quad (\text{S78})$$

$$\hat{S}_j^- |N/2, m\rangle = \frac{1}{2} \sqrt{(N/2-m+1)(N/2+m)} |N/2, m-1\rangle + \frac{(-1)^j}{2} \sqrt{\frac{(N/2+m)(N/2+m-1)}{N-1}} |N/2-1, m-1\rangle. \quad (\text{S79})$$

Now we consider a general initial state in the collective manifold,

$$|\psi_0\rangle = \sum_m c_m |N/2, m\rangle, \quad (\text{S80})$$

with the constraints $\langle \psi_0 | \hat{S}_n^y | \psi_0 \rangle = 0$, $\langle \psi_0 | \hat{S}_n^z | \psi_0 \rangle = 0$. With time evolution under \hat{H}_{eff} , we have

$$\begin{aligned} |\psi(t)\rangle &= e^{-i\hat{H}_{\text{eff}}t/\hbar} \\ &\approx \sum_m c_m \left[e^{-iN J_{\text{eff}}t/2} |N/2, m\rangle - i \frac{\omega_{\text{eff}}}{N J_{\text{eff}}} \sqrt{\frac{(N/2)^2 - m^2}{N-1}} \sin(N J_{\text{eff}}t/2) |N/2 - 1, m\rangle \right], \end{aligned} \quad (\text{S81})$$

which gives

$$\begin{aligned} \langle \psi(t) | \hat{S}_j^+ | \psi(t) \rangle &\approx \sum_m c_m c_{m+1}^* \left[\langle N/2, m+1 | \hat{S}_j^+ | N/2, m \rangle \right. \\ &\quad - i \frac{\omega_{\text{eff}}}{N J_{\text{eff}}} e^{iN J_{\text{eff}}t/2} \sqrt{\frac{(N/2)^2 - m^2}{N-1}} \sin(N J_{\text{eff}}t/2) \langle N/2, m+1 | \hat{S}_j^+ | N/2 - 1, m \rangle \\ &\quad \left. + i \frac{\omega_{\text{eff}}}{N J_{\text{eff}}} e^{-iN J_{\text{eff}}t/2} \sqrt{\frac{(N/2)^2 - (m+1)^2}{N-1}} \sin(N J_{\text{eff}}t/2) \langle N/2 - 1, m+1 | \hat{S}_j^+ | N/2, m \rangle \right] \\ &= \sum_m c_m c_{m+1}^* \langle N/2, m+1 | \hat{S}_j^+ | N/2, m \rangle \left[1 - (-1)^j \frac{\omega_{\text{eff}}}{N J_{\text{eff}}} \left(i \frac{1}{2} \sin(N J_{\text{eff}}t) - \frac{2m+1}{N-1} \sin^2(N J_{\text{eff}}t/2) \right) \right] \\ &= \langle \psi_0 | \hat{S}_j^+ | \psi_0 \rangle \left[1 - i(-1)^j \frac{\omega_{\text{eff}}}{2} \frac{\sin(N J_{\text{eff}}t)}{N J_{\text{eff}}} \right] + \frac{\langle \psi_0 | (\hat{S}_n^+ \hat{S}^z + \hat{S}^z \hat{S}_n^+) | \psi_0 \rangle}{N-1} (-1)^j \frac{\omega_{\text{eff}}}{N J_{\text{eff}}} \sin^2(N J_{\text{eff}}t/2). \end{aligned} \quad (\text{S82})$$

Therefore, we can obtain the frequency for each of the two large spins,

$$\omega_j(t) \approx (-1)^{j-1} \frac{\omega_{\text{eff}}}{2} \left(\frac{\sin(N J_{\text{eff}}t)}{N J_{\text{eff}}t} - 2 \frac{\langle \psi_0 | (\hat{S}^y \hat{S}^z + \hat{S}^z \hat{S}^y) | \psi_0 \rangle \sin^2(N J_{\text{eff}}t/2)}{(N-1) \langle \psi_0 | \hat{S}^x | \psi_0 \rangle N J_{\text{eff}}t} \right), \quad (\text{S83})$$

leading to the synchronization time

$$N J_{\text{eff}} t_{\text{syn}} = \pi - 2 \arctan \left[\frac{\langle \psi_0 | (\hat{S}^y \hat{S}^z + \hat{S}^z \hat{S}^y) | \psi_0 \rangle}{(N-1) \langle \psi_0 | \hat{S}^x | \psi_0 \rangle} \right]. \quad (\text{S84})$$

In the following, we consider three different types of initial states:

- $|\psi_0\rangle = |+\rangle^{\otimes N}$

In this case we have $\langle \psi_0 | (\hat{S}^y \hat{S}^z + \hat{S}^z \hat{S}^y) | \psi_0 \rangle = 0$, which gives

$$N J_{\text{eff}} t_{\text{syn},0} = \pi. \quad (\text{S85})$$

Here we use $t_{\text{syn},0}$ to label the synchronization time with this unentangled initial state. This result agrees with the prediction using the Holstein–Primakoff approximation in the previous subsection.

- $|\psi_0\rangle = e^{-iQ\hat{S}^z/N} |+\rangle^{\otimes N}$

In this case we have

$$\langle \psi_0 | (\hat{S}^y \hat{S}^z + \hat{S}^z \hat{S}^y) | \psi_0 \rangle = \frac{N(N-1)}{2} \sin(Q/N) \cos^{N-2}(Q/N), \quad (\text{S86})$$

$$\langle \psi_0 | \hat{S}^x | \psi_0 \rangle = \frac{N}{2} \cos^{N-1}(Q/N), \quad (\text{S87})$$

which gives

$$N J_{\text{eff}} t_{\text{syn}} = \pi - 2Q/N. \quad (\text{S88})$$

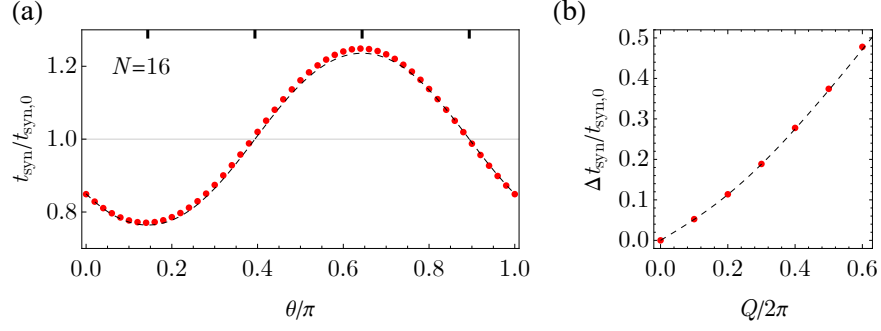


Fig. S6. Comparison between numerical simulations of superexchange interactions \hat{H}_{SE} with $N = 16$ atoms in a single tube and analytic results Eq. (S92) and Eq. (S93). We use the same protocol as Fig. 4 in the main text. (a) The dependence of synchronization time on the rotation $\hat{R}_x^\theta = \exp(-i\theta\hat{S}^x)$ at $Q/2\pi = 0.6$. (b) The dependence of the tunable range of synchronization time on OAT shearing strength Q .

Note that the $\hat{S}^z\hat{S}^z$ term commutes with \hat{H}_{eff} , this result can also apply to the following Hamiltonian generated by cavity-mediated interactions,

$$\hat{H}_{\text{cav}}/\hbar = J_\perp \hat{\mathbf{S}} \cdot \hat{\mathbf{S}} + (J_z - J_\perp) \hat{S}^z \hat{S}^z + \frac{\omega_{\text{eff}}}{2} (\hat{S}_1^z - \hat{S}_2^z), \quad (\text{S89})$$

with initial state $|\psi_0\rangle = |+\rangle^{\otimes N}$. Now we can replace J_{eff} by J_\perp , and Q/N by $(J_z - J_\perp)t_{\text{syn}}$, which gives

$$\left((N-2)J_\perp + 2J_z \right) t_{\text{syn}} = \pi. \quad (\text{S90})$$

We have shown numerical calculations for collective spin exchange interactions ($J_z = 0$) and collective Heisenberg interactions ($J_z = J_\perp$) for a 1D tube with N atoms in Fig. S5(b), which agrees well with the analytic results using two large spins.

- $|\psi_0\rangle = e^{-i\theta\hat{S}^x} e^{-iQ\hat{S}^z\hat{S}^z/N} |+\rangle^{\otimes N}$

In this case we have

$$\langle \psi_0 | (\hat{S}^y \hat{S}^z + \hat{S}^z \hat{S}^y) | \psi_0 \rangle = \cos(2\theta) \frac{N(N-1)}{2} \sin(Q/N) \cos^{N-2}(Q/N) + \sin(2\theta) \frac{N(N-1)}{8} \left(1 - \cos^{N-2}(2Q/N) \right), \quad (\text{S91})$$

and $\langle \psi_0 | \hat{S}^x | \psi_0 \rangle$ is still given by Eq. (S87). So the tunability of synchronization time is due to the θ -rotation of $\langle \psi_0 | (\hat{S}^y \hat{S}^z + \hat{S}^z \hat{S}^y) | \psi_0 \rangle$. In Fig. 4 of the main text and Fig. S6, we find that the analytic results for two large spins can also explain the numerical simulations for collective or nearest-neighbor Heisenberg interactions, if we rewrite the formula of synchronization time t_{syn} and its tunable range Δt_{syn} into dimensionless form,

$$\frac{t_{\text{syn}}}{t_{\text{syn},0}} = 1 - \frac{2}{\pi} \arctan \left[\frac{\langle \psi_0 | (\hat{S}^y \hat{S}^z + \hat{S}^z \hat{S}^y) | \psi_0 \rangle}{(N-1) \langle \psi_0 | \hat{S}^x | \psi_0 \rangle} \right], \quad (\text{S92})$$

$$\frac{\Delta t_{\text{syn}}}{t_{\text{syn},0}} = \frac{4}{\pi} \arctan \left[\frac{\left(\langle \psi_0 | (\hat{S}^y \hat{S}^z + \hat{S}^z \hat{S}^y) | \psi_0 \rangle \right)_{\text{max}}}{(N-1) \langle \psi_0 | \hat{S}^x | \psi_0 \rangle} \right]. \quad (\text{S93})$$

In the main text, we use $|\psi(\theta)\rangle$ instead of $|\psi_0\rangle$ in this case to emphasize the θ -dependence.

[S1] C. M. Will, *Theory and experiment in gravitational physics* (Cambridge university press, 2018).

[S2] P. K. Schwartz and D. Giulini, Post-newtonian hamiltonian description of an atom in a weak gravitational field, *Physical Review A* **100**, 052116 (2019).

- [S3] V. J. Martínez-Lahuerta, S. Eilers, T. E. Mehlstäubler, P. O. Schmidt, and K. Hammerer, Ab initio quantum theory of mass defect and time dilation in trapped-ion optical clocks, *Physical Review A* **106**, 032803 (2022).
- [S4] M. Werner, P. K. Schwartz, J.-N. Kirsten-Siemß, N. Gaaloul, D. Giulini, and K. Hammerer, Atom interferometers in weakly curved spacetimes using bragg diffraction and bloch oscillations, *Phys. Rev. D* **109**, 022008 (2024).
- [S5] F. E. Close and H. Osborn, Relativistic center-of-mass motion and the electromagnetic interaction of systems of charged particles, *Physical Review D* **2**, 2127 (1970).
- [S6] T. Bothwell, C. J. Kennedy, A. Aeppli, D. Kedar, J. M. Robinson, E. Oelker, A. Staron, and J. Ye, Resolving the gravitational redshift across a millimetre-scale atomic sample, *Nature* **602**, 420 (2022).
- [S7] A. Aeppli, A. Chu, T. Bothwell, C. J. Kennedy, D. Kedar, P. He, A. M. Rey, and J. Ye, Hamiltonian engineering of spin-orbit-coupled fermions in a wannier-stark optical lattice clock, *Science Advances* **8**, eadc9242 (2022).
- [S8] M. Sonnleitner and S. M. Barnett, Mass-energy and anomalous friction in quantum optics, *Physical Review A* **98**, 042106 (2018).
- [S9] M. A. Norcia, R. J. Lewis-Swan, J. R. Cline, B. Zhu, A. M. Rey, and J. K. Thompson, Cavity-mediated collective spin-exchange interactions in a strontium superradiant laser, *Science* **361**, 259 (2018).
- [S10] X. Zhang, M. Bishof, S. L. Bromley, C. V. Kraus, M. S. Safronova, P. Zoller, A. M. Rey, and J. Ye, Spectroscopic observation of su (n)-symmetric interactions in sr orbital magnetism, *Science* **345**, 1467 (2014).
- [S11] G. F. Gribakin and V. V. Flambaum, Calculation of the scattering length in atomic collisions using the semiclassical approximation, *Physical Review A* **48**, 546 (1993).
- [S12] A. Goban, R. B. Hutson, G. E. Marti, S. L. Campbell, M. A. Perlin, P. S. Julienne, J. P. D’incio, A. M. Rey, and J. Ye, Emergence of multi-body interactions in a fermionic lattice clock, *Nature* **563**, 369 (2018).
- [S13] M. A. Perlin and A. M. Rey, Effective multi-body su (n)-symmetric interactions of ultracold fermionic atoms on a 3d lattice, *New Journal of Physics* **21**, 043039 (2019).
- [S14] A. Piñeiro Orioli, J. K. Thompson, and A. M. Rey, Emergent dark states from superradiant dynamics in multilevel atoms in a cavity, *Physical Review X* **12**, 011054 (2022).
- [S15] A. Chu, A. Piñeiro Orioli, D. Barberena, J. K. Thompson, and A. M. Rey, Photon-mediated correlated hopping in a synthetic ladder, *Physical Review Research* **5**, L022034 (2023).
- [S16] W. R. Milner, S. Lannig, M. Mamaev, L. Yan, A. Chu, B. Lewis, M. N. Frankel, R. B. Hutson, A. M. Rey, and J. Ye, Coherent evolution of superexchange interaction in seconds long optical clock spectroscopy, arXiv:2402.13398 (2024).